3.06 Earth Tides

D. C. Agnew, University of California San Diego, San Diego, CA, USA

3.06.1 Introduction

The Earth tides are the motions induced in the solid Earth, and the changes in its gravitational potential, induced by the tidal forces from external bodies. (These forces, acting on the rotating Earth, also induce motions of its spin axis, treated in Chapter 3.10). Tidal fluctuations have three roles in geophysics: measurements of them can provide information about the Earth; models of them can be used to remove tidal variations from measurements of something else; and the same models can be used to examine tidal influence on some phenomenon. An example of the first role would be measuring the nearly diurnal resonance in the gravity tide to estimate the flattening of the core–mantle boundary (CMB); of the second, computing the expected tidal displacements at a point so we can better estimate its position with the Global Positioning System (GPS); and of the third, finding the tidal stresses to see if they trigger earthquakes. The last two activities are possible because the Earth tides are relatively easy to model quite accurately; in particular, these are much easier to model than the ocean tides are, both because the Earth is more rigid than water, and because the geometry of the problem is much simpler.

For modeling the tides it is an advantage that they can be computed accurately, but an unavoidable consequence of such accuracy is that it is difficult to use Earth-tide measurements to find out about the Earth. The Earth's response to the tides can be

described well with only a few parameters; even knowing those few parameters very well does not provide much information. This was not always true; in particular, in 1922 Jeffreys used tidal data to show that the average rigidity of the Earth was much less than that of the mantle, indicating that the core must be of very low rigidity (Brush, 1996). But subsequently, seismology has determined Earth structure in much more detail than could be found with tides. Recently, Earth tides have become more important in geodesy, as the increasing precision of measurements has required corrections for tidal effects that could previously be ignored, This chapter therefore focuses on the theory needed to compute tidal effects as accurately as possible, with less attention to tidal data or measurement techniques; though of course the theory is equally useful for interpreting tidal data, or phenomena possibly influenced by tides.

There are a number of reviews of Earth tides available; the best short introduction remains that of Baker (1984). Melchior (1983) describes the subject fully (and with a very complete bibliography), but is now somewhat out of date, and should be used with caution by the newcomer to the field. The volume of articles edited by Wilhelm *et al.* (1997) is a better reflection of the current state of the subject, as are the quadrennial *International Symposia on Earth Tides* (e.g., Jentzsch, 2006). Harrison (1985) reprints a number of important papers, with very thoughtful commentary; Cartwright (1999) is a history of tidal science (mostly the ocean tides) that also provides an interesting introduction to some aspects of the field – which, as one of the older parts of geophysics, has a terminology sometimes overly affected by history.

3.06.1.1 An Overview

Figure 1 is a simple flowchart to indicate what goes into a tidal signal. We usually take the tidal forcing to be completely known, but it is computed using a particular theory of gravity, and it is actually the case that Earth-tide measurements provide some of the best evidence available for general relativity as opposed to some other alternative theories (Warburton and Goodkind, 1976). The large box labeled Geophysics/oceanography includes the response of the Earth and ocean to the forcing, with the arrow going around it to show that some tides would be observed even if the Earth were oceanless and rigid. Finally, measurements of Earth tides can detect other environmental and tectonic signals.

At this point it is useful to introduce some terminology. The 'theoretical tides' could be called the modeled tides, since they are computed from a set of models. The first model is the tidal forcing, or 'equilibrium tidal potential', produced by external bodies; this is computed from gravitational and astronomical theory, and is the tide at point E in **Figure 1**. The next two models are those that describe how the Earth and ocean respond to this forcing; in **Figure 1** these are boxes inside the large dashed box. The solid-Earth model gives what are called the 'body tides', which are what would be observed on an oceanless but otherwise realistic Earth. The ocean model (which includes both the oceans and the elastic Earth) gives the 'load tides', which are changes in the solid Earth caused by the shifting mass of water associated with the ocean tides. These two responses sum to give the total tide

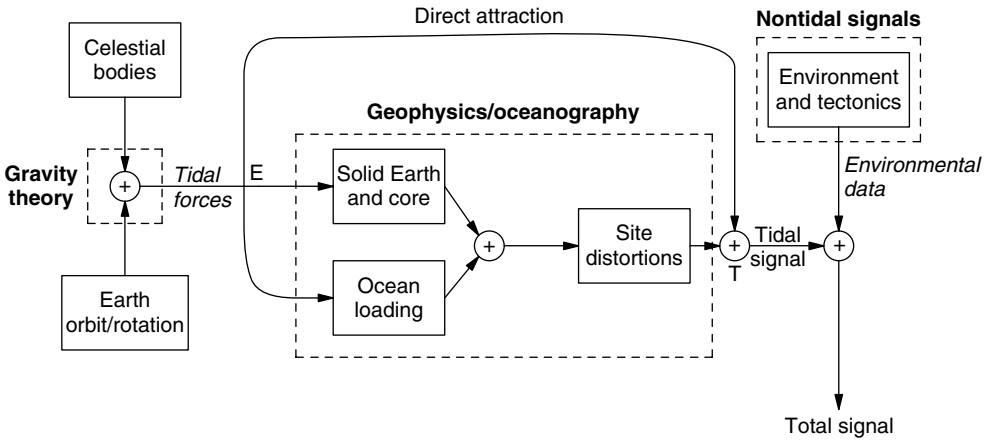

Figure 1 Tidal flowchart. Entries in italics represent things we know (or think we know) to very high accuracy; entries in boldface (over the dashed boxes) represent things we can learn about using tidal data. See text for details.

caused by the nonrigidity of the Earth; the final model, labeled 'site distortions', may be used to describe how local departures from idealized models affect the result (Section 3.06.6.1). This nonrigid contribution is summed with the tide from direct attraction to give the total theoretical tide, at point T in the flowchart.

Mathematically, we can describe the processes shown on this flowchart in terms of linear systems, something first applied to tidal theory by Munk and Cartwright (1966). The total signal $y(t)$ is represented by

$$y(t) = \int x_T(t-\tau) w_T(\tau) d\tau + n(t) \qquad [1]$$

where $x_T(t)$ is the tidal forcing and $n(t)$ is the noise (nontidal energy, from whatever source). The function $w(t)$ is the impulse response of the system to the tidal forcing. Fourier transforming eqn [1], and disregarding the noise, gives $Y(f) = W_T(f) X_T(f)$: $W(f)$ is the 'tidal admittance', which turns out to be more useful than $w(t)$, partly because of the bandlimited nature of X_T, but also because (with one exception) $W(f)$ turns out to be a fairly smooth function of frequency. To predict the tides we assume $W(f)$ (perhaps guided by previous measurements); to analyze them, we determine $W(f)$.

We describe the tidal forcing first, in some detail because the nature of this forcing governs the response and how tidal measurements are analyzed. We next consider how the solid Earth responds to the tidal forcing, and what effects this produces. After this we discuss the load tides, completing what we need to know to produce the full theoretical tides. We conclude with brief descriptions of analysis methods appropriate to Earth-tide data, and instruments for measuring Earth tides.

3.06.2 The Tidal Forces

The tidal forces arise from the gravitational attraction of bodies external to the Earth. As noted above, computing them requires only some gravitational potential theory and astronomy, with almost no geophysics. The extraordinarily high accuracy of astronomical theory makes it easy to describe the tidal forcing to much more precision than can be measured: perhaps as a result, in this part of the subject the romance of the next decimal place has exerted a somewhat excessive pull.

Our formal derivation of the tidal forcing will use potential theory, but it is useful to start by considering the gravitational forces exerted on one body (the Earth, in this case) by another. As usual in discussing gravitation, we work in terms of accelerations. Put most simply, the tidal acceleration at a point on or in the Earth is the difference between the acceleration caused by the attraction of the external body and the orbital acceleration – which is to say, the acceleration which the Earth undergoes as a whole. This result is valid whatever the nature of the orbit – it would hold just as well if the Earth were falling directly toward another body. For a spherically symmetric Earth the orbital acceleration is the acceleration caused by the attraction of the other body at the Earth's center of mass, making the tidal force the difference between the attraction at the center of mass, and that at the point of observation.

Figure 2 shows the resulting force field. At the point directly under the attracting body (the 'sub-body point'), and at its antipode, the tidal force is oppositely directed in space, though in the same way (up) viewed from the Earth. It is in fact larger at the sub-body point than at its antipode, though if the ratio a/R is small (1/60 for the forces plotted in **Figure 2**) the difference is also small.

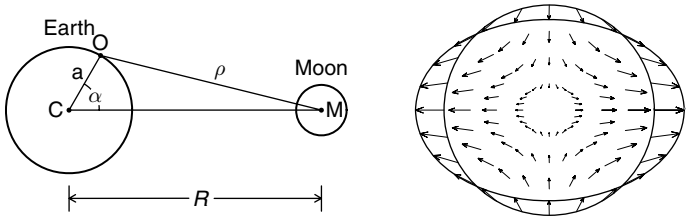

Figure 2 Tidal forcing. On the left is the geometry of the problem for computing the tidal force at a point *O* on the Earth, given an external body M. The right plot shows the field of forces (accelerations) for the actual Earth–Moon separation; the scale of the largest arrow is 1.14 $\mu m\,s^{-2}$ for the Moon, and 0.51 $\mu m\,s^{-2}$ for the Sun. The elliptical line shows the equipotential surface under tidal forcing, greatly exaggerated.

3.06.2.1 The Tidal Potential

We now derive an expression for the tidal force – or rather, for the more useful 'tidal potential', following the development in Munk and Cartwright (1966). If M_{ext} is the mass of the external body, the gravitational potential, V_{tot}, from it at O is

$$V_{\text{tot}} = \frac{GM_{\text{ext}}}{\rho} = \frac{GM_{\text{ext}}}{R}\frac{1}{\sqrt{1+(a/R)^2-2(a/R)\cos\alpha}}$$

using the cosine rule from trigonometry. The variables are as shown in **Figure 2**: a is the distance of O from C, ρ the distance from O to M, and α the angular distance between O and the sub-body point of M. We can write the square-root term as a sum of Legendre polynomials, using the generating-function expression for these, which yields

$$V_{\text{tot}} = \frac{GM_{\text{ext}}}{R}\sum_{n=0}^{\infty}\left(\frac{a}{R}\right)^n P_n(\cos\alpha) \qquad [2]$$

where $P_2(x) = (1/2)(3x^2-1)$ and $P_3(x) = (1/2)(5x^3-3x)$.

The $n=0$ term is constant in space, so its gradient (the force) is zero, and it can be discarded. The $n=1$ term is

$$\frac{GM_{\text{ext}}}{R^2}a\cos\alpha = \frac{GM_{\text{ext}}}{R^2}x_1 \qquad [3]$$

where x_1 is the Cartesian coordinate along the C–M axis. The gradient of this is a constant, corresponding to a constant force along the direction to M; but this is just the orbital force at C, which we subtract to get the tidal force. Thus, the tidal potential is eqn [2] with the two lowest terms removed:

$$V_{\text{tid}}(t) = \frac{GM_{\text{ext}}}{R(t)}\sum_{n=2}^{\infty}\left(\frac{a}{R(t)}\right)^n P_n[\cos\alpha(t)] \qquad [4]$$

where we have made R and α, as they actually are, functions of time t – which makes V such a function as well.

We can now put in some numbers appropriate to the Earth and relevant external bodies to get a sense of the magnitudes of different terms. If r is the radius of the Earth, $a/R = 1/60$ for the Moon, so that the size of terms in the sum [4] decreases fairly rapidly with increasing n; in practice, we need to only consider $n=2$ and $n=3$, and perhaps $n=4$ for the highest precision; the $n=4$ tides are just detectable in very low noise gravimeters. These different values of n are referred to as the degree-n tides. For the Sun, $r/R = 1/23\,000$, so the degree-2 solar tides completely dominate.

If we consider $n=2$, the magnitude of V_{tid} is proportional to GM_{ext}/R^3. If we normalize this quantity to make the value for the Moon equal to 1, the value for the Sun is 0.46, for Venus 5×10^{-5}, and for Jupiter 6×10^{-6}, and even less for all other planets. So the 'lunisolar' tides dominate, and are probably the only ones visible in actual measurements – though, as we will see, some expansions of the tidal potential include planetary tides.

At very high precision, we also need to consider another small effect: the acceleration of the Earth is exactly equal to the attraction of the external body at the center of mass only for a spherically symmetric Earth. For the real Earth, the C_{20} term in the gravitational potential makes the acceleration of the Moon by the Earth (and hence the acceleration of the Earth by the Moon) depend on more than just eqn [3]. The resulting Earth-flattening tides (Wilhelm, 1983; Dahlen, 1993) are however small.

We can get further insight on the behavior of the tidal forces if we use geographical coordinates, rather than angular distance from the sub-body point. Suppose our observation point O is at colatitude θ and east longitude ϕ (which are fixed) and that the sub-body point of M is at colatitude $\theta'(t)$ and east longitude $\phi'(t)$. Then we may apply the addition theorem for spherical harmonics to get, instead of [4],

$$V_{\text{tid}} = \frac{GM_{\text{ext}}}{R(t)}\sum_{n=2}^{\infty}\left(\frac{a}{R(t)}\right)^n\frac{4\pi}{2n+1} \times\sum_{m=-n}^{n}Y^*_{nm}(\theta'(t),\phi'(t))\,Y_{nm}(\theta,\phi) \qquad [5]$$

where we have used the fully normalized complex spherical harmonics defined by

$$Y_{nm}(\theta,\,\phi) = N_n^m P_n^m(\cos\theta)\mathrm{e}^{\mathrm{i}m\phi}$$

where

$$N_n^m = (-1)^m\left[\frac{2n+1}{4\pi}\frac{(n-m)!}{(n+m)!}\right]^{1/2}$$

is the normalizing factor and P_n^m is the associated Legendre polynomial of degree n and order m (**Table 1**).

Table 1 Associated Legendre functions

$P_2^0(\theta) = \frac{1}{2}(3\cos^2\theta-1)$	$P_3^0(\theta) = \frac{1}{2}(5\cos^3\theta-3\cos\theta)$
$P_2^1(\theta) = 3\sin\theta\cos\theta$	$P_3^1(\theta) = \frac{3}{2}(5\cos^2\theta-1)$
$P_2^2(\theta) = 3\sin^2\theta$	$P_3^2(\theta) = 15\sin^2\theta\cos\theta$
	$P_3^3(\theta) = 15\sin^3\theta$

As is conventional, we express the tidal potential as V_{tid}/g, where g is the Earth's gravitational acceleration; this combination has the dimension of length, and can easily be interpreted as the change in elevation of the geoid, or of an equilibrium surface such as an ideal ocean (hence its name, the 'equilibrium potential'). Part of the convention is to take g to have its value on the Earth's equatorial radius a_{eq}; if we hold r fixed at that radius in [5], we get

$$\begin{aligned}\frac{V_{\text{tid}}}{g} &= a_{\text{eq}}\frac{M_{\text{ext}}}{M_{\text{E}}}\sum_{n=2}^{\infty}\frac{4\pi}{2n+1}\left(\frac{a_{\text{eq}}}{R}\right)^{n+1}\\ &\quad\times\sum_{m=-n}^{n}Y_{nm}^{*}(\theta',\,\phi')\,Y_{nm}(\theta,\,\phi)\\ &= \sum_{n=2}^{\infty}K_n\frac{4\pi}{2n+1}\xi^{n+1}\\ &\quad\times\sum_{m=-n}^{n}Y_{nm}^{*}(\theta',\,\phi')\,Y_{nm}(\theta,\,\phi)\end{aligned}\qquad[6]$$

where the constant K includes all the physical quantities:

$$K_n = a_{\text{eq}}\frac{M_{\text{ext}}}{M_{\text{E}}}\left(\frac{a_{\text{eq}}}{\overline{R}}\right)^{n+1}$$

where M_{E} is the mass of the Earth and $\overline{R}$ is the mean distance of the body; the quantity $\xi = \overline{R}/R$ expresses the normalized change in distance. For the Moon, K_2 is 0.35837 m, and for the Sun, 0.16458 m.

In both [5] and [6], we have been thinking of θ and ϕ as giving the location of a particular place of observation; but if we consider them to be variables, the $Y_{nm}(\theta, \phi)$ describes the geographical distribution of V/g on the Earth. The time dependence of the tidal potential comes from time variations in R, θ', and ϕ'. The first two change relatively slowly because of the orbital motion of M around the Earth; ϕ' varies approximately daily as the Earth rotates beneath M. The individual terms in the sum over m in [6] thus separate the tidal potential of degree n into parts, called 'tidal species', that vary with frequencies around 0, 1, 2, ..., n times per day; for the largest tides ($n = 2$), there are three such species. The diurnal tidal potential varies once per day, and with colatitude as $\sin\theta\,\cos\theta$: it is largest at mid-latitudes and vanishes at the equator and the poles. The semidiurnal part (twice per day) varies as $\sin^2\theta$ and so is largest at the equator and vanishes at the poles. The long-period tide varies as $3\cos^2\theta - 1$, and so is large at the pole and (with reversed sign) at the equator. As we will see, these spatial dependences do not carry over to those tides, such as strain and tilt, that depend on horizontal gradients of the potential.

To proceed further it is useful to separate the time-dependent and space-dependent parts a bit more explicitly. We adopt the approach of Cartwright and Tayler (1971) who produced what was, for a long time, the standard harmonic expansion of the tidal potential. We can write [6] as

$$\begin{aligned}\frac{V_{\text{tid}}}{g} &= \sum_{n=2}^{\infty}K_n\xi^{n+1}\frac{4\pi}{2n+1}\left[Y_{n0}(\theta',\,\phi')\,Y_{n0}(\theta,\,\phi)\right.\\ &\quad+\sum_{m=1}^{n}Y_{n-m}^{*}(\theta',\,\phi')\,Y_{n-m}(\theta,\,\phi)\\ &\quad\left.+\,Y_{nm}^{*}(\theta',\,\phi')\,Y_{nm}(\theta,\,\phi)\right]\\ &= \sum_{n=2}^{\infty}K_n\xi^{n+1}\frac{4\pi}{2n+1}\left[Y_{n0}(\theta',\,\phi')\,Y_{no}(\theta,\,\phi)\right.\\ &\quad\left.+\sum_{m=1}^{n}2\Re\left[Y_{nm}^{*}(\theta',\,\phi')\,Y_{nm}(\theta,\,\phi)\right]\right]\end{aligned}$$

Now define complex (and time-varying) coefficients $T_{nm}(t) = a_n^m(t) + \mathrm{i}b_n^m(t)$ such that

$$\frac{V_{\text{tid}}}{g} = \Re\left[\sum_{n=2}^{\infty}\sum_{m=0}^{n}T_{nm}^{*}(t)\,Y_{nm}(\theta,\,\phi)\right]\qquad[7]$$

$$\begin{aligned}&= \sum_{n=2}^{n=\infty}\sum_{m=0}^{n}N_n^m P_n^m(\cos\theta)[a_n^m(t)\cos m\phi\\ &\quad+ b_n^m(t)\sin m\phi]\end{aligned}\qquad[8]$$

Then the T_{nm} coefficients are, for m equal to 0,

$$T_{n0} = \left(\frac{4\pi}{2n+1}\right)^{1/2}K_n\xi^{n+1}P_n^0(\cos\theta')\qquad[9]$$

and, for m not equal to 0,

$$T_{nm} = (-1)^m\frac{8\pi}{2n+1}K_n\xi^{n+1}N_n^m P_n^m(\theta')\mathrm{e}^{\mathrm{i}\phi'}\qquad[10]$$

from which we can find the real-valued, time-varying quantities $a_n^m(t)$ and $b_n^m(t)$, which we will use below in computing the response of the Earth.

3.06.2.2 Computing the Tides: Direct Computation

Equations [7]–[10] suggest a straightforward way to compute the tidal potential (and, as we will see, other theoretical tides). First, use a description of the location of the Moon and Sun in celestial coordinates (an ephemeris); other planets can be included if we wish. Then convert this celestial location to the geographical coordinates θ' and ϕ' of the sub-body point, and the distance R, using standard transformations (McCarthy and Pétit, 2004, Chapter 4). Finally,

use eqns [9] and [10] to get $T_{nm}(t)$. Once we have the T_{nm}, we can combine these with the spatial factors in [7] to get V_{tid}/g, either for a specific location or as a distribution over the whole Earth. As we will see, we can vary the spatial factors to find, not just the potential, but other observables, including tilt and strain, all with no changes to the T_{nm}; we need to do the astronomy only once.

A direct computation has the advantage, compared with the harmonic methods (discussed below) of being limited in accuracy only by the accuracy of the ephemeris. If we take derivatives of [10] with respect to R, θ', and ϕ', we find that relative errors of 10^{-4} in V_{tid}/g would be caused by errors of 7×10^{-5} rad (14″) in θ' and ϕ', and 3×10^{-5} in ξ. (We pick this level of error because it usually exceeds the accuracy with which the tides can be measured, either because of noise or because of instrument calibration.) The errors in the angular quantities correspond to errors of about 400 m in the location of the sub-body point, so our model of Earth rotation, and our station location, needs to be good to this level – which requires 1 s accuracy in the timing of the data.

Two types of ephemerides are available: analytical, which provide a closed-form algebraic description of the motion of the body; and the much more precise numerical ephemerides, computed from numerical integration of the equations of motion, with parameters chosen to best fit astronomical data. While numerical ephemerides are more accurate, they are less convenient for most users, being available only as tables; analytical ephemerides are or can be made available as computer code.

The first tidal-computation program based directly on an ephemeris was that of Longman (1959), still in use for making rough tidal corrections for gravity surveys. Longman's program, like some others, computed accelerations directly, thus somewhat obscuring the utility of an ephemeris-based approach to all tidal computations. Munk and Cartwright (1966) applied this method for the tidal potential. Subsequent programs such as those of Harrison (1971), Broucke *et al.* (1972), Tamura (1982), and Merriam (1992) used even more precise ephemerides based on subsets of Brown's lunar theory.

Numerical ephemerides have been used primarily to produce reference time series, rather than for general-purpose programs, although the current IERS standards use such a method for computing tidal potentials and displacements (with corrections described in Section 3.06.3.2.2). Most precise calculations (e.g., Hartmann and Wenzel, 1995) have relied on the numerical ephemerides produced by JPL (Standish *et al.*, 1992). The resulting tidal series form the basis for a harmonic expansion of the tidal potential, a standard method to which we now turn.

3.06.2.3 Computing the Tides (I): Harmonic Decompositions

Since the work of Thomson and Darwin in the 1870s and 1880s, the most common method of analyzing and predicting the tides, and of expressing tidal behavior, has been through a 'harmonic expansion' of the tidal potential. In this, we express the T_{nm} as a sum of sinusoids, whose frequencies are related to combinations of astronomical frequencies and whose amplitudes are determined from the expressions in the ephemerides for R, θ', and ϕ'. In such an expansion, we write the complex T_{nm}'s as

$$T_{nm}(t) = \sum_{k=1}^{K_{nm}} A_{knm} \exp[i(2\pi f_{knm} t + \varphi_{knm})] \qquad [11]$$

where, for each degree and order we sum K_{nm} sinusoids with specified real amplitudes, frequencies, and phases A, f, and φ. The individual sinusoids are called 'tidal harmonics' (not the same as the spherical harmonics of Section 3.06.2.1).

This method has the conceptual advantage of decoupling the tidal potential from the details of astronomy, and the practical advantage that a table of harmonic amplitudes and frequencies, once produced, is valid over a long time. Such an expansion also implicitly puts the description into the frequency domain, something as useful here as in other parts of geophysics. We can use the same frequencies for any tidal phenomenon, provided that it comes from a linear response to the driving potential – which is essentially true for the Earth tides. So, while this expansion was first used for ocean tides (for which it remains the standard), it works just as well for Earth tides of any type.

To get the flavor of this approach, and also introduce some terminology, we consider tides from a very simple situation: a body moving at constant speed β in a circular orbit, the orbital plane being inclined at an angle ε to the Earth's equator. The angular distance from the ascending node (where the orbit plane and the equatorial plane intersect) is βt. The rotation of the Earth, at rate Ω, causes the terrestrial longitude of the ascending node to be Ωt; since the ascending node is fixed in space, Ω corresponds to one revolution per sidereal day. We further assume that at $t = 0$ the body is at the ascending node

and longitude 0° is under it. Finally, we take just the real part of [6], and do not worry about signs.

With these simplifications we consider first the diurnal degree-2 tides ($n=2$, $m=1$). After some tedious spherical trigonometry and algebra, we find that

$$V/g = K_2\left(\frac{6\pi}{5}\right)[\sin\varepsilon\cos\varepsilon\sin\Omega t + \frac{1}{2}\sin\varepsilon(1+\cos\varepsilon)\sin(\Omega-2\beta)t + \frac{1}{2}\sin\varepsilon(1-\cos\varepsilon)\sin(\Omega+2\beta)t]$$

This shows that the harmonic decomposition includes three harmonics, with arguments (of time) Ω, $\Omega-2\beta$, and $\Omega+2\beta$; their amplitudes depend on ε, the inclination of the orbital plane. If ε were zero, there would be no diurnal tides at all. For our simple model, a reasonable value of ε is 23.44°, the inclination of the Sun's orbital plane, and the mean inclination of the Moon's. These numbers produce the harmonics given in **Table 2**, in which the frequencies are given in cycles per solar day (cpd). Both the Moon and Sun produce a harmonic at 1 cycle per sidereal day. For the Moon, β corresponds to a period of 27.32 days (the tropical month) and for the Sun 365.242 days (one year), so the other harmonics are at ±2 cycles per month, or ±2 cycles per year, from this. Note that there is not a harmonic at 1 cycle per lunar (or solar) day – this is not unexpected, given the degree-2 nature of the tidal potential.

It is convenient to have a shorthand way of referring to these harmonics; unfortunately the standard naming system, now totally entrenched, was begun by Thomson for a few tides, and then extended by Darwin in a somewhat *ad hoc* manner. The result is a series of conventional names that simply have to be learned as is (though only the ones for the largest tides are really important). For the Moon, the three harmonics have the Darwin symbols K_1, O_1, and OO_1; for the Sun they are K_1 (again, since this has the same frequency for any body), P_1, and ϕ_1.

For the semidiurnal ($m=2$ case), the result is

$$V/g = K_2\left(\frac{24\pi}{5}\right)[(1-\cos^2\varepsilon)\cos2\Omega t + \frac{1}{2}(1+\cos\varepsilon)^2\times\cos(2\Omega-2\beta)t + \frac{1}{2}(1-\cos\varepsilon)^2\cos(2\Omega+2\beta)t]$$

again giving three harmonics, though for ε equal to 23.44°, the third one is very small. Ignoring the last term, we have two harmonics, also listed in **Table 2**. The Darwin symbol for the first argument is K_2; again, this frequency is the same for the Sun and the Moon, so these combine to make a lunisolar tide. The second argument gives the largest tides: for the Moon, M_2 (for the Moon) or S_2 (for the Sun), at precisely 2 cycles per lunar (or solar) day, respectively.

Finally, the $m=0$, or long-period, case has

$$V/g = K_2\left(\frac{\pi}{5}\right)\left[\left(1.5\sin^2\varepsilon-1\right)-1.5\sin^2\varepsilon\cos2\beta t\right]$$

which gives one harmonic at zero frequency (the so-called 'permanent tide'), and another with an argument of 2β, making tides with frequencies of 2 cycles per month (Mf, the fortnightly tide, from the Moon) and 2 cycles per year (Ssa, the semiannual tide, from the Sun).

This simple model demonstrates another important attribute of the tides, arising from the dependence on the orbital inclination ε. For the Sun this is nearly invariant, but for the Moon it varies

Table 2 Tidal constituents (simple model)

Argument	Moon		Sun	
	Freq. (cpd)	Amp. (m)	Freq. (cpd)	Amp. (m)
Long-period tides				
	0.000000	0.217	0.000000	0.100
2β	0.073202	0.066	0.005476	0.030
Diurnal tides				
Ω	1.002738	0.254	1.002738	0.117
$\Omega-2\beta$	0.929536	0.265	0.997262	0.122
$\Omega+2\beta$	1.075940	0.011	1.008214	0.005
Semidiurnal tides				
2Ω	2.005476	0.055	2.005476	0.025
$2\Omega-2\beta$	1.932274	0.640	2.000000	0.294

by $\pm 5.13^\circ$ from the mean, with a period of 18.61 years. This produces a variation in amplitude in all the lunar tides, which is called the 'nodal modulation'. The simple expressions show that the resulting variation is $\pm 18\%$ for O_1, and $\pm 3\%$ for M_2. Such a modulated sinusoid can be written as $\cos\omega_0 t(1 + A\cos\omega_m t)$, with $\omega_0 \gg \omega_m$; this is equal to

$$\cos\omega_0 t + \frac{1}{2}A\cos[(\omega_0 + \omega_m)t] + \frac{1}{2}A\cos[(\omega_0 - \omega_m)t]$$

so we can retain a development purely in terms of sinusoids, but with three harmonics, one at the central frequency and two smaller ones (called 'satellite harmonics') separated from it by 1 cycle in 18.61 years.

An accurate ephemeris would include the ellipticity of the orbits, and all the periodic variations in ε and other orbital parameters, leading to many harmonics; for a detailed description, see Bartels (1957/1985). The first full expansion, including satellite harmonics, was by Doodson (1921), done algebraically from an analytical ephemeris; the result had 378 harmonics. Doodson needed a nomenclature for these tides, and introduced one that relies on the fact that, as our simple ephemeris suggests, the frequency of any harmonic is the sum of multiples of a few basic frequencies. For any (n, m), we can write the argument of the exponent in [11] as

$$2\pi f_k t + \phi_k = \left(\sum_{l=1}^{6} D_{lk} 2\pi f_l\right) t + \sum_{l=1}^{6} D_{lk}\varphi_l$$

where the f_l's are the frequencies corresponding to various astronomical periods, and the φ_l's are the phases of these at some suitable epoch; **Table 3** gives a list. (Recent tabulations extend this notation with up to five more arguments to describe the motions of the planets. As the tides from these are small we ignore them here.) The $l = 1$ frequency is chosen to be one cycle per lunar day exactly, so for the M_2 tide the D_l's are $2, 0, 0, 0, 0, 0$. This makes the solar tide, S_2, have the D_l's $2, 2, 2, 0, 0, 0$. In practice, all but the smallest tides have D_{lk} ranging from -5 to 5 for $l > 1$. Doodson therefore added 5 to these numbers to make a compact code, so that M_2 becomes 255·555 and S_2 273·555. This is called the Doodson number; the numbers without 5 added are sometimes called Cartwright–Tayler codes (**Table 4**).

Figure 3 shows the full spectrum of amplitude coefficients, from the recent expansion of Hartmann and Wenzel (1995). The top panel shows all harmonics on a linear scale, making it clear that only a few are large, and the separation into different species around 0, 1, and 2 cycles/day: these are referred to as the long-period, diurnal, and semidiurnal tidal bands. The two lower panels show an expanded view of the diurnal and semidiurnal bands, using a log scale of amplitude to include the smaller harmonics. What is apparent from these is that each tidal species is split into a set of bands, separated by 1 cycle/month; these are referred to as 'groups': in each group the first two digits of the Doodson number are the same. All harmonics with the same first three digits of the Doodson number are in clusters separated by 1 cycle/year; these clusters are called 'constituents', though this name is also sometimes used for the individual harmonics. As a practical matter this is usually the finest frequency resolution attainable; on the scale of this plot finer frequency separations, such as the nodal modulation, are visible only as a thickening of some of the lines. All this fine-scale structure poses a challenge to tidal analysis methods (Section 3.06.5.1).

Since Doodson provided the tidal potential to more than adequate accuracy for studying ocean tides, further developments did not take place for the next 50 years, until Cartwright and Tayler (1971) revisited the subject. Using eqn [6], they computed the potential from a more modern lunar ephemeris, and then applied special Fourier methods to analyze, numerically, the resulting series, and get amplitudes for the various harmonics. The result was

Table 3 Fundamental tidal frequencies

l	Symbol	Frequency (cycles/day)	Period	What
1	τ	0.9661368	24 h 50 m 28.3 s	Lunar day
2	s	0.0366011	27.3216 d	Moon's longitude: tropical month
3	h	0.0027379	365.2422 d	Sun's longitude: solar year
4	p	0.0003095	8.847 yr	Lunar perigee
5	N'	0.0001471	18.613 yr	Lunar node
6	p_s	0.0000001	20941 yr	Solar perigee

Longitude refers to celestial longitude, measured along the ecliptic.

Table 4 Largest tidal harmonics, for $n = 2$, sorted by size for each species

Amplitude (m)	Doodson number	Frequency (cpd)	Darwin symbol
Long-period tides			
−0.31459	055.555	0.0000000	M_0, S_0
−0.06661	075.555	0.0732022	Mf
−0.03518	065.455	0.0362916	Mm
−0.03099	057.555	0.0054758	Ssa
0.02793	055.565	0.0001471	*N*
−0.02762	075.565	0.0733493	
−0.01275	085.455	0.1094938	Mtm
−0.00673	063.655	0.0314347	MSm
−0.00584	073.555	0.0677264	MSf
−0.00529	085.465	0.1096409	
Diurnal tides			
0.36864	165.555	1.0027379	K_1
−0.26223	145.555	0.9295357	O_1
−0.12199	163.555	0.9972621	P_1
−0.05021	135.655	0.8932441	Q_1
0.05003	165.565	1.0028850	
−0.04947	145.545	0.9293886	
0.02062	175.455	1.0390296	J_1
0.02061	155.655	0.9664463	M_1
0.01128	185.555	1.0759401	OO_1
−0.00953	137.455	0.8981010	ρ_1
−0.00947	135.645	0.8930970	
−0.00801	127.555	0.8618093	σ_1
0.00741	155.455	0.9658274	
−0.00730	165.545	1.0025908	
0.00723	185.565	1.0760872	
−0.00713	162.556	0.9945243	π_1
−0.00664	125.755	0.8569524	$2Q_1$
0.00525	167.555	1.0082137	ϕ_1
Semidiurnal tides			
0.63221	255.555	1.9322736	M_2
0.29411	273.555	2.0000000	S_2
0.12105	245.655	1.8959820	N_2
0.07991	275.555	2.0054758	K_2
0.02382	275.565	2.0056229	
−0.02359	255.545	1.9321265	
0.02299	247.455	1.9008389	ν_2
0.01933	237.555	1.8645472	μ_2
−0.01787	265.455	1.9685653	L_2
0.01719	272.556	1.9972622	T_2
0.01602	235.755	1.8596903	$2N_2$
0.00467	227.655	1.8282556	ε_2
−0.00466	263.655	1.9637084	λ_2

a compendium of 505 harmonics, which (with errors corrected by Cartwright and Edden (1973)) soon became the standard under the usual name of the CTE representation. (A few small harmonics at the edges of each band, included by Doodson but omitted by Cartwright, are sometimes added to make a CTED list with 524 harmonics.)

More extensive computations of the tidal potential and its harmonic decomposition have been driven by the very high precision available from the ephemerides and the desire for more precision for analyzing some tidal data (gravity tides from superconducting gravimeters). Particular expansions are those of Bullesfeld (1985), Tamura (1987), Xi (1987), Hartmann and Wenzel (1995), and Roosbeek (1995) . The latest is that of Kudryavtsev (2004) , with 27 000 harmonics. **Figure 4** shows the amplitude versus number of harmonics; to get very

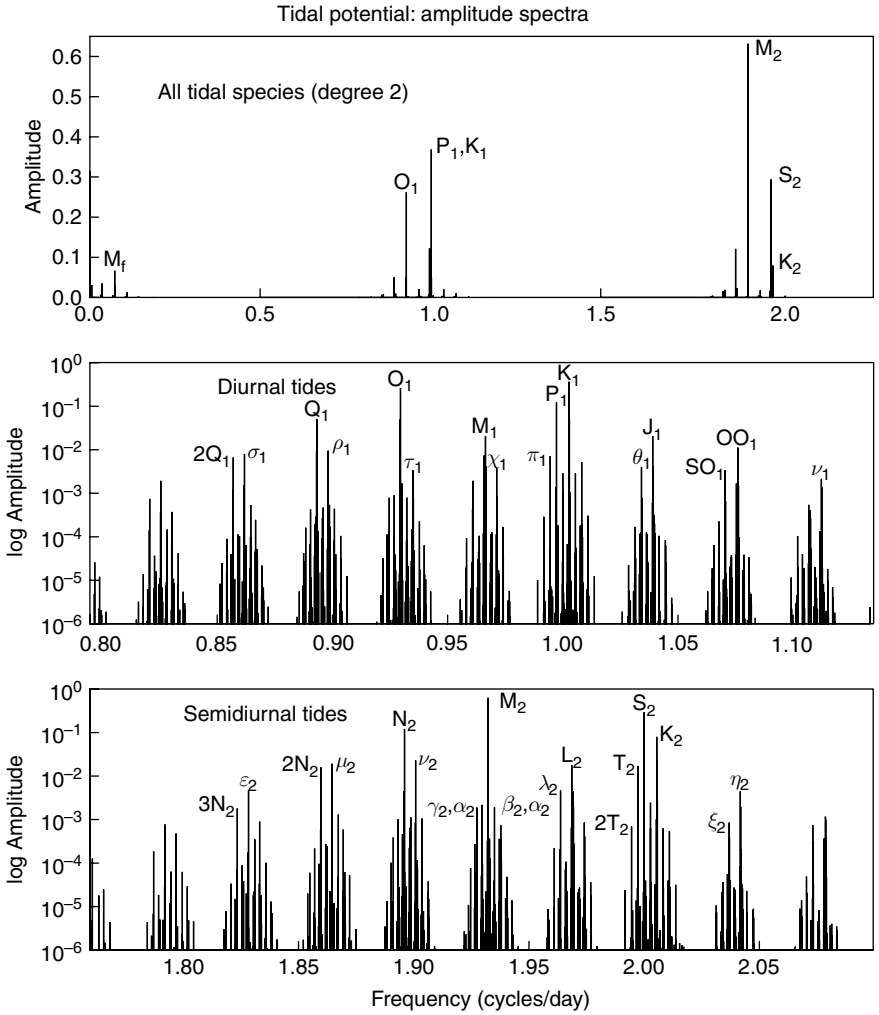

Figure 3 The spectrum of the tidal potential. Since all variations are purely sinusoidal, the spectrum is given by the amplitudes of the tidal harmonics, taken from Hartmann and Wenzel (1995), though normalized according to the convention of Cartwright and Tayler (1971). The Darwin symbols are shown for the larger harmonics (top) and all named diurnal and semidiurnal harmonics, except for a few that are shown only in **Figure 5**.

high accuracy demands a very large number. But not many are needed for a close approximation; the CTED expansion is good to about 0.1% of the total tide.

3.06.2.4 The Pole Tide

Both in our elementary discussion and in our mathematical development of the tidal forcing, we treated the Earth's rotation only as a source of motion of the sub-body point. But changes in this rotation also cause spatial variations in the gravitational potential, and since these have the same effects as the attraction of external bodies, they can also be regarded as tides. The only significant one is the 'pole tide', which is caused by changes in the direction of the Earth's spin axis relative to a point fixed in the Earth. The spin produces a centrifugal force, which depends on the angular distance between the spin axis and a location. As the spin axis moves, this distance, and the centrifugal force, changes.

Mathematically, the potential at a location $\mathbf{r}$ from a spin vector $\boldsymbol{\Omega}$ is

$$V = \frac{1}{2}\left[|\boldsymbol{\Omega}|^2|\mathbf{r}|^2 - |\boldsymbol{\Omega}\cdot\mathbf{r}|^2\right] \qquad [12]$$

We assume that the rotation vector is nearly along the 3-axis, so that we have $\boldsymbol{\Omega} = \Omega(m_1\hat{\mathbf{x}}_1 + m_2\hat{\mathbf{x}}_2 + \hat{\mathbf{x}}_3)$,

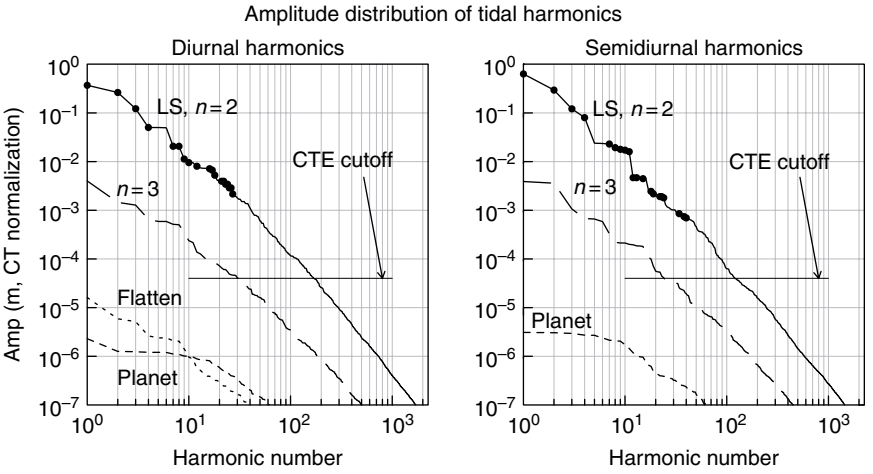

Figure 4 Distribution of harmonic amplitudes for the catalog of Hartmann and Wenzel (1995) , normalized according to Cartwright and Tayler (1971). The line 'LS, $n=2$' refers to lunisolar harmonics of degree 2; those with large dots have Darwin symbols associated with them. Constituents of degree 3, from other planets, and from earth flattening are shown as separate distributions. The horizontal line shows the approximate cutoff level of the Cartwright and Tayler (1971) list.

with m_1 and m_2 both much less than 1. If we put this expression into [12], and subtract V for m_1 and m_2 both zero, the potential height for the pole tide is

$$\frac{V}{g} = -\frac{\Omega^2}{2g}[2(m_1 r_1 r_3 + m_2 r_2 r_3)]$$
$$= -\frac{\Omega^2 a^2}{g}\sin\theta\cos\theta(m_1\cos\phi + m_2\sin\phi)$$

This is a degree-2 change in the potential, of the same form as for the diurnal tides. However, the periods involved are very different, since the largest pole tides come from the largest polar motions, at periods of 14 months (the Chandler wobble) and 1 year. The maximum range of potential height is a few cm, small but not negligible; pole-tide signals have been observed in sea-level data and in very precise gravity measurements. This 'tide' is now usually allowed for in displacement measurements, being computed from the observed polar motions (Wahr, 1985). The accompanying ocean tide is marginally observable (Haubrich and Munk, 1959; Miller and Wunsch, 1973; Trupin and Wahr, 1990; Desai, 2002).

3.06.2.5 Radiational Tides

The harmonic treatment used for the gravitational tides can also be useful for the various phenomena associated with solar heating. The actual heating is complicated, but a first approximation is to the input radiation, which is roughly proportional to the cosine of the Sun's elevation during the day and zero at night; Munk and Cartwright (1966) called this the 'radiational tide'. The day–night asymmetry produces harmonics of degrees 1 and 2; these have been tabulated by Cartwright and Tayler (1971) and are shown in **Figure 5** as crosses (for both degrees), along with the tidal potential harmonics shown as in **Figure 3**. The unit for the radiational tides is S, the solar constant, which is 1366 W m $^{-2}$.

These changes in solar irradiation drive changes in ground temperature fairly directly, and changes in air temperature and pressure in very complicated ways. Ground-temperature changes cause thermoelastic deformations with tidal periods (Berger, 1975; Harrison and Herbst, 1977; Mueller, 1977). Air pressure changes, usually known as 'atmospheric tides' (Chapman and Lindzen, 1970), load the Earth enough to cause deformations and changes in gravity. Such effects are usually treated as noise, but the availability of better models of some of the atmospheric tides (Ray, 2001; Ray and Ponte, 2003; Ray and Poulose, 2005) and their inclusion in ocean-tide models (Ray and Egbert, 2004) has allowed their effects to be compared with gravity observations (Boy *et al.*, 2006b).

That some of these thermal tidal lines coincide with lines in the tidal potential poses a real difficulty for precise analysis of the latter. Strictly speaking, if we have the sum of two harmonics with the same frequency, it will be impossible to tell how much each part contributes. The only way to resolve this is to make additional assumptions about how the response to these behaves at other frequencies. Even

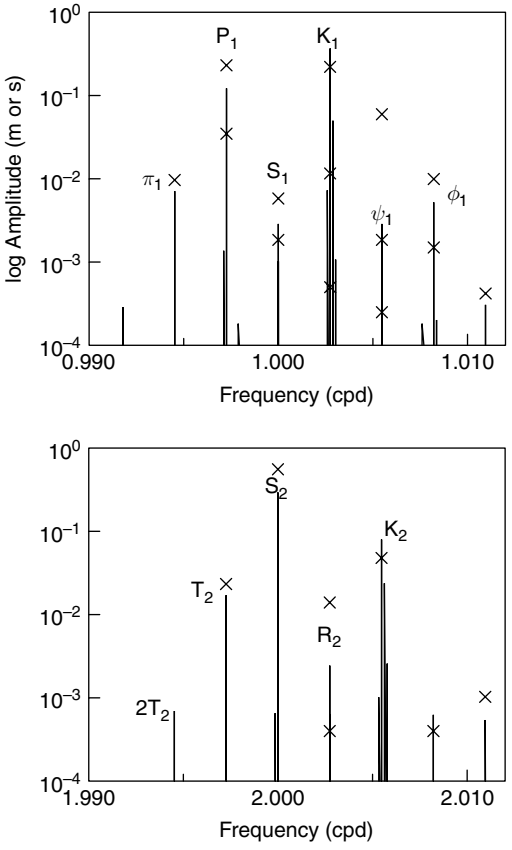

Figure 5 Radiational tides. The crosses show the amplitudes of the radiational tidal harmonics (degree 1 and 2) from Cartwright and Tayler (1971); the amplitudes are for the solar constant S being taken to be 1.0. The lines are harmonics of the gravitational tides, as in **Figure 3**.

when this is done, there is a strong likelihood that estimates of these tides will have large systematic errors – which is why, for example, the large K_1 tide is less used in estimating tidal responses than the smaller O_1 tide is.

3.06.3 Tidal Response of the Solid Earth

Having described the tidal forces, we next turn to the response of the solid Earth – which, as is conventional, we assume to be oceanless, putting in the effect of the ocean tides at a later step. We start with the usual approximation of a spherical Earth in order to introduce a number of concepts, many of them adequate for all but the most precise modeling of the tides. We then describe what effects a better approximation has, in enough detail to enable computation; the relevant theory is beyond the scope of this treatment, though outlined in Chapter 3.10.

3.06.3.1 Tidal Response of a SNREI Earth

To a good approximation, we can model the tidal response of an oceanless Earth by assuming a SNREI Earth model: that is, one that is **S**pherical, **N**on-**R**otating, **E**lastic, and **I**sotropic. As in normal-mode seismology (from which this acronym comes), this means that the only variation of elastic properties is with depth. In addition to these restrictions on the Earth model, we add one more about the tidal forcing: that it has a much longer period than any normal modes of oscillation of the Earth so that we can use a quasi-static theory, taking the response to be an equilibrium one. Since the longest-period normal modes for such an Earth have periods of less than an hour, this is a good approximation.

It is simple to describe the response of a SNREI Earth to the tidal potential (Jeffreys, 1976). Because of symmetry, only the degree n is relevant. If the potential height at a point on the surface is $V(\theta, \phi)/g$, the distortion of the Earth from tidal forces produces an additional gravitational potential $k_n V(\theta, \phi)$, a vertical (i.e., radial) displacement $h_n V(\theta, \phi)/g$, and a horizontal displacement $l_n(\nabla_1 V(\theta, \phi)/g)$, where ∇_1 is the horizontal gradient operator on the sphere. So defined, k_n h_n, and l_n are dimensionless; they are called Love numbers, after A. E. H. Love (though the parameter l_n was actually introduced by T. Shida). For a standard modern earth model (PREM) $h_2 = 0.6032$, $k_2 = 0.2980$, and $l_2 = 0.0839$. For comparison, the values for the much older Gutenberg–Bullen Earth model are 0.6114, 0.3040, and 0.0832 – not very different. In this section we adopt values for a and g that correspond to a spherical Earth: 6.3707×10^6 m and 9.821 m s^{-2}, respectively.

3.06.3.1.1 Some combinations of Love numbers (I): gravity and tilt

Until there were data from space geodesy, neither the potential nor the displacements could be measured; what could be measured were ocean tides, tilt, changes in gravity, and local deformation (strain), each of which possessed its own expression in terms of Love numbers – which we now derive. Since the first three of these would exist even on a rigid Earth, it is common to describe them using the ratio between what they are on an elastic Earth (or on the real Earth) and what they would be on a rigid Earth.

The simplest case is that of the effective tide-raising potential: that is, the one relevant to the ocean tide. The total tide-raising potential height is $(1+k_n)V/g$, but the solid Earth (on which a tide gauge sits) goes up by h_nV/g, so the effective tide-raising potential is $(1+k_n-h_n)V/g$, sometimes written as γ_nV/g, γ_n being called the 'diminishing factor'. For the PREM model $\gamma_2=0.6948$. Since tilt is just the change in slope of an equipotential surface, again relative to the deforming solid Earth, it scales in the same way that the potential does: the tilt on a SNREI Earth is γ_n times the tilt on a rigid Earth. The NS tilt is, using eqn [8] and expressions for the derivatives of Legendre functions,

$$\begin{aligned}\lambda_N &= \frac{-\gamma_n}{ga}\frac{\partial V}{\partial\theta}\\ &= \frac{-1}{a\sin\theta}\sum_{n=2}^{n=\infty}\gamma_n\sum_{m=0}^{n}N_n^m[n\cos\theta P_n^m(\cos\theta)-(n+m)\\ &\quad\times P_{n-1}^m(\cos\theta)][a_n^m(t)\cos m\phi+b_n^m(t)\sin m\phi]\end{aligned}\qquad[13]$$

where the sign is chosen such that a positive tilt to the North would cause a plumb line to move in that direction. The East tilt is

$$\begin{aligned}\lambda_E &= \frac{\gamma_n}{ga\sin\theta}\frac{\partial V}{\partial\phi}=\frac{-1}{a\sin\theta}\sum_{n=2}^{n=\infty}\gamma_n\sum_{m=0}^{n}mN_n^mP_n^m(\cos\theta)\\ &\quad\times[b_n^m(t)\cos m\phi-a_n^m(t)\sin m\phi]\end{aligned}\qquad[14]$$

with the different combinations of a and b with the ϕ dependence showing that this tilt is phase-shifted relative to the potential, by 90° if we use a harmonic decomposition.

Tidal variations in gravity were for a long time the commonest type of Earth-tide data. For a spherical Earth, the tidal potential is, for degree n,

$$V_n\left(\frac{r}{a}\right)^n+k_nV_n\left(\frac{a}{r}\right)^{n+1}$$

where the first term is the potential caused by the tidal forcing (and for which we have absorbed all nonradial dependence into V_n), and the second is the additional potential induced by the Earth's deformation. The corresponding change in local gravitational acceleration is the radial derivative of the potential:

$$\frac{\partial}{\partial r}\left[V_n\left(\left(\frac{r}{a}\right)^n+k_n\left(\frac{a}{r}\right)^{n+1}\right)\right]_{r=a}=V_n\left[\frac{n}{a}-(n+1)\frac{k_n}{a}\right]\qquad[15]$$

In addition to this change in gravity from the change in the potential, there is a change from the gravimeter being moved up by an amount h_nV_n/g. The change in gravity is this displacement times the gradient of g, $2g/a$, plus the displacement times $-\omega^2$, where ω is the radian frequency of the tidal motion – that is, the inertial acceleration. (We adopt the Earth-tide convention that a decrease in g is positive.) If we ignore this last part (which is at most 1.5% of the gravity-gradient part), we get a total change of

$$V_n\left[\frac{n}{a}-\left(\frac{n+1}{a}\right)k_n+\frac{2h_n}{a}\right]=\frac{nV_n}{a}\left[1-\left(\frac{n+1}{n}\right)k_n+\frac{2}{n}h_n\right]\qquad[16]$$

The nV_n/a term is the change in g that would be observed on a rigid Earth (with h and k zero); the term which this is multiplied by, namely

$$\delta_n=1+\frac{2h_n}{n}-\left(\frac{n+1}{n}\right)k_n$$

is called the 'gravimetric factor'. For the PREM model, $\delta_2=1.1562$: the gravity tides are only about 16% larger than they would be on a completely rigid Earth, so that most of the tidal gravity signal shows only that the Moon and Sun exist, but does not provide any information about the Earth. The expression for the gravity tide is of course very similar to eqn [8]:

$$\begin{aligned}\delta g &= \frac{g}{a}\sum_{n=2}^{n=\infty}\delta_n\sum_{m=0}^{n}N_n^mP_n^m(\cos\theta)[a_n^m(t)\cos m\phi\\ &\quad+b_n^m(t)\sin m\phi]\end{aligned}\qquad[17]$$

3.06.3.1.2 Combinations of Love numbers (II): displacement and strain tides

For a tidal potential of degree n, the displacements at the surface of the Earth ($r=a$) will be, by the definitions of the Love numbers l_n and h_n,

$$u_r=\frac{h_nV}{g},\qquad u_\theta=\frac{l_n}{g}\frac{\partial V}{\partial\theta},\qquad u_\phi=\frac{l_n}{g\sin\theta}\frac{\partial V}{\partial\phi}\qquad[18]$$

in spherical coordinates. Comparing these with [17], [13], and [14], we see that the vertical displacement is exactly proportional to changes in gravity, with the scaling constant being $h_na/2\delta_ng=1.692\times10^5\,s^2$; and that the horizontal displacements are exactly proportional to tilts, with the scaling constant being $l_na/\gamma_n=7.692\times10^5$ m; we can thus use eqns [17], [13], and [14], suitably scaled, to find tidal displacements.

Taking the derivatives of [18], we find the tensor components of the surface strain are

$$e_{\theta\theta} = \frac{1}{ga}\left(h_n V + l_n \frac{\partial^2 V}{\partial^2 \theta}\right)$$

$$e_{\phi\phi} = \frac{1}{ga}\left(h_n V + l_n \cot\theta \frac{\partial V}{\partial \theta} + \frac{l_n}{\sin\theta}\frac{\partial^2 V}{\partial^2 \phi}\right)$$

$$e_{\theta\phi} = \frac{l_n}{ga\sin\theta}\left(\frac{\partial^2 V}{\partial\theta\partial\phi} - \cot\theta \frac{\partial V}{\partial\phi}\right)$$

We again use [8] for the tidal potential, and get the following expressions that give the formulas for the three components of surface strain for a particular n and m; to compute the total strain these should be summed over all $n \geq 2$ and all m from 0 to n (though in practice the strain tides with $n > 3$ or $m = 0$ are unobservable).

$$\begin{aligned} e_{\theta\theta} = {} & \frac{N_n^m}{a\sin^2\theta}\left[\left(h_n \sin^2\theta + l_n\left(n^2\cos^2\theta - n\right)\right)P_n^m(\cos\theta)\right. \\ & -2l_n(n-1)(n+m)\cos\theta P_{n-1}^m(\cos\theta) \\ & \left. + l_n(n+m)(n+m-1)P_{n-2}^m(\cos\theta)\right] \\ & \times \left[a_n^m(t)\cos m\phi + b_n^m(t)\sin m\phi\right] \end{aligned}$$

$$\begin{aligned} e_{\phi\phi} = {} & \frac{N_n^m}{a\sin^2\theta}\left[\left(h_n \sin^2\theta + l_n\left(n\cos^2\theta - m^2\right)\right)P_n^m(\cos\theta)\right. \\ & \left. - l_n(n+m)\cos\theta P_{n-1}^m(\cos\theta)\right] \\ & \times \left[a_n^m(t)\cos m\phi + b_n^m(t)\sin m\phi\right] \end{aligned}$$

$$\begin{aligned} e_{\theta\phi} = {} & \frac{mN_n^m l_n}{a\sin^2\theta}\left[(n-1)\cos\theta P_n^m(\cos\theta) - (n+m)P_{n-1}^m(\cos\theta)\right] \\ & \times \left[b_n^m(t)\cos m\phi - a_n^m(t)\sin m\phi\right] \end{aligned}$$

Note that the combination of the longitude factors with the $a_n^m(t)$ and $b_n^m(t)$ means that $e_{\theta\theta}$ and $e_{\phi\phi}$ are in phase with the potential, while $e_{\theta\phi}$ is not.

One consequence of these expressions is that, for $n = 2$ and m equal to either 1 or 2, the areal strain, $(1/2)(e_{\theta\theta} + e_{\phi\phi})$, is equal to $V(h_2 - 3l_2)/ga$: areal strain, vertical displacement, the potential, and gravity are all scaled versions of each other. Close to the surface, the free-surface condition means that deformation is nearly that of plane stress, so vertical and volume strains are also proportional to areal strain, and likewise just a scaled version of the potential.

If we combine these expressions for spatial variation with the known amplitudes of the tidal forces, we can see how the rms amplitude of the body tides varies with latitude and direction (**Figure 6**). There are some complications in the latitude dependence; for example, the EW semidiurnal strain tides go to zero at 52.4° latitude. Note that while the tilt tides are larger than strain tides, most of this signal is from the direct attractions of the Sun and Moon; the purely deformational part of the tilt is about the same size as the strain.

3.06.3.2 Response of a Rotating Earth

We now turn to models for tides on an oceanless and isotropic Earth, still with properties that depend on depth only, but add rotation and slightly inelastic behavior. Such models have three consequences for the tides:

1. The ellipticity of the CMB and the rotation of the Earth combine to produce a free oscillation in which the fluid core (restrained by pressure forces) and solid mantle precess around each other. This is known as the 'nearly diurnal free wobble' (NDFW) or 'free core nutation'. Its frequency falls within the band of the diurnal tides, which causes a resonant response in the Love numbers near 1 cycle/day. The diurnal tides also cause changes in the direction of the Earth's spin axis (the astronomical precessions and nutations), and the NDFW affects these as well, so that some of the best data on it come from astronomy (Herring *et al.*, 2002).
2. Ellipticity and rotation couple the response to forcing of degree n to spherical harmonics of other degrees, and spheroidal to toroidal modes of deformation. As a result, the Love numbers become slightly latitude dependent, and additional terms appear for horizontal displacement.
3. The imperfect elasticity of the mantle (finite Q) modifies the Love numbers in two ways: they become complex, with small imaginary parts; and they become weakly frequency dependent because of anelastic dispersion.

The full theory for these effects, especially the first two, is quite complicated. Love (1911) provided some theory for the effects of ellipticity and rotation, and Jeffreys and Vincente (1957) and Molodenskii (1961) for the NDFW, but the modern approach for these theories was described by Wahr (1981a, 1981b); a simplified version is given by Neuberg *et al.* (1987) and Zürn (1997). For more recent developments, see the article by Dehant and Mathews in this volume, and Mathews *et al.* (1995a, 1995b, 1997, 2002), Wang (1997), Dehant *et al.* (1999), and Mathews and Guo (2005).

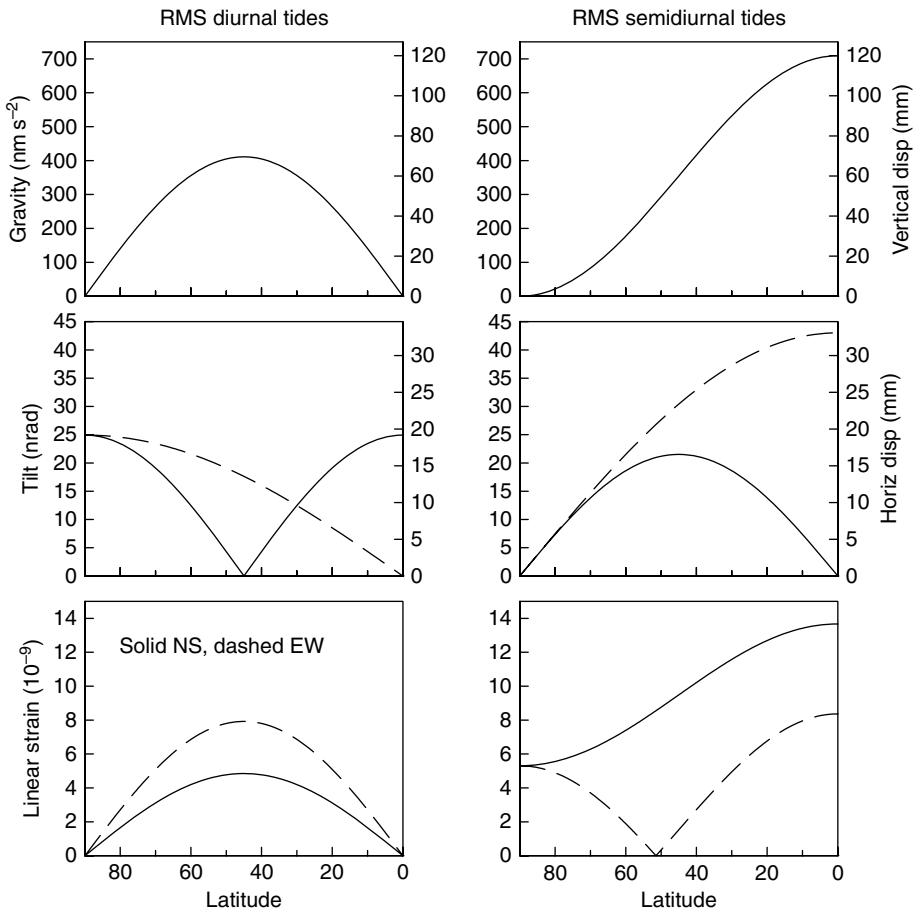

Figure 6 RMS tides. The left plots show the rms tides in the diurnal band, and the right plots the rms in the semidiurnal band. The uppermost frame shows gravity and vertical displacement (with scales for each) which have the same latitude dependence; the next horizontal displacement and tilt; and the bottom linear strain. In all plots but the top, dashed is for EW measurements, solid for NS.

To obtain the full accuracy of these theories, particularly for the NDFW correction, requires the use of tabulated values of the Love numbers for specific harmonics, but analytical approximations are also available. The next three sections outline these, using values from the IERS standards (McCarthy and Pétit, 2004) for the Love numbers and from Dehant *et al.* (1999) for the gravimetric factor.

3.06.3.2.1 NDFW resonance

The most important result to come out of the combination of improved theoretical development and observations has been that the period of the NDFW, both in the Earth tides and in the nutation, is significantly different from that originally predicted. The NDFW period is in part controlled by the ellipticity of the CMB, which was initially assumed to be that for a hydrostatic Earth. The observed period difference implies that the ellipticity of the CMB departs from a hydrostatic value by about 5%, the equivalent of a 500 m difference in radius, an amount not detectable using seismic data. This departure is generally thought to reflect distortion of the CMB by mantle convection.

The resonant behavior of the Love numbers from the NDFW is confined to the diurnal band; within that band it can be approximated by an expansion in terms of the resonant frequencies:

$$L(f) = S_z + \sum_{k=1}^{2} \frac{S_k}{f - f_k} \qquad [19]$$

where $L(f)$ is the frequency-dependent Love number (of whatever type) for frequency f in cycles per solar day; The expansion in use for the IERS standards includes three resonances: the Chandler wobble, the NDFW, and the free inner core nutation

Table 5 Coefficients (real and imaginary parts) used in eqn [19] to find the frequency dependence of the Love numbers (including corrections for ellipticity) in the diurnal tidal band

	$R(S_z)$	$I(S_z)$	$R(S_1)$	$I(S_1)$	$R(S_2)$	$I(S_2)$
δ_0	1.15802	0.0	-2.871×10^{-3}	0.0	4.732×10^{-5}	0.0
$k^{(0)}$	0.29954	-1.412×10^{-3}	-7.811×10^{-4}	-3.721×10^{-5}	9.121×10^{-5}	-2.971×10^{-6}
$h^{(0)}$	0.60671	-2.420×10^{-3}	-1.582×10^{-3}	-7.651×10^{-5}	1.810×10^{-4}	-6.309×10^{-6}
$l^{(0)}$	0.08496	-7.395×10^{-4}	-2.217×10^{-4}	-9.672×10^{-6}	-5.486×10^{-6}	-2.998×10^{-7}
δ_+	1.270×10^{-4}	0.0	-2.364×10^{-5}	0.0	1.564×10^{-6}	0.0
k^+	-8.040×10^{-4}	2.370×10^{-6}	2.090×10^{-6}	1.030×10–7	-1.820×10^{-7}	6.500×10^{-9}
$h^{(2)}$	-6.150×10^{-4}	-1.220×10^{-5}	1.604×10^{-6}	1.163×10^{-7}	2.016×10^{-7}	2.798×10^{-9}
$l^{(2)}$	1.933×10^{-4}	-3.819×10^{-6}	-5.047×10^{-7}	-1.643×10^{-8}	-6.664×10^{-9}	5.090×10^{-10}
$l^{(1)}$	1.210×10^{-3}	1.360×10^{-7}	-3.169×10^{-6}	-1.665×10^{-7}	2.727×10^{-7}	-8.603×10^{-9}
l^P	-2.210×10^{-4}	-4.740×10^{-8}	5.776×10^{-7}	3.038×10^{-8}	1.284×10^{-7}	-3.790×10^{-9}

(FICN); to a good approximation (better than 1%), the last can be ignored. **Table 5** gives the values of the S's according to the IERS standards (and to Dehant *et al.* (1999) for the gravimetric factors), scaled for f in cycles per solar day; in these units the resonance frequencies are

$$f_1 = -2.60812 \times 10^{-3} - 1.365 \times 10^{-4} i$$
$$f_2 = 1.0050624 + 2.5 \times 10^{-5} i$$

and the FICN frequency (not used in [19]) is $1.00176124 + 7.82 \times 10^{-4} i$. Dehant *et al.* (1999) use purely real-valued frequencies, with $f_1 = -2.492 \times 10^{-3}$ and $f_2 = 1.0050623$, as well as purely real values of the S's.

Figure 7 shows the NDFW resonance, for a signal (areal strain) relatively sensitive to it. Unfortunately, the tidal harmonics do not sample the resonance very well; the largest effect is for the small ψ_1 harmonic, which is also affected by radiational tides. While tidal measurements (Zürn, 1997) have confirmed the frequency shift seen in the nutation data, the latter at this time seem to give more precise estimates of the resonant behavior.

One consequence of the NDFW resonance is that we cannot use equations of the form [17] to compute the theoretical diurnal tides, since the factor for them varies with frequency. If we construct the $a_n^m(t)$ and $b_n^m(t)$ using [11], it is easy to adjust the harmonic amplitudes and phases appropriately. Alternatively, if we find $a_n^m(t)$ and $b_n^m(t)$ using an ephemeris, we can compute the diurnal tides assuming a frequency-independent factor, and then apply corrections for

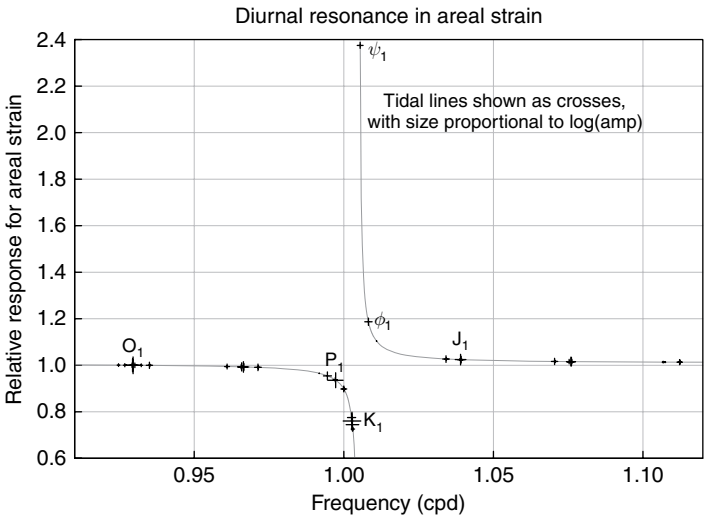

Figure 7 NDFW response, for the combination of Love numbers that gives the areal strain, normalized to 1 for the O_1 tide. The crosses show the locations of tidal harmonics, with size of symbol proportional to the logarithm of the amplitude of the harmonic.

the few harmonics that are both large and affected by the resonance; Mathews *et al.* (1997) and McCarthy and Pétit (2004) describe such a procedure for displacements and for the induced potential.

3.06.3.2.2 Coupling to other modes

The other effect of rotation and ellipticity is to couple the spheroidal deformation of degree n, driven by the potential, to spheroidal deformations of degree $n \pm 2$ and toroidal deformations of degree $n \pm 1$. Thus, the response to the degree-2 part of the tidal potential contains a small component of degrees 0 and 4. If we generalize the Love numbers, describing the response as a ratio between the response and the potential, the result will be a ratio that depends on latitude: we say that the Love number has become latitude dependent.

Such a generalization raises issues of normalization; unlike the spherical case, the potential and the response may be evaluated on different surfaces. This has been a source of some confusion. The normalization of Mathews *et al.* (1995b) is the one generally used for displacements: it uses the response in displacement on the surface of the ellipsoid, but takes these to be relative to the potential evaluated on a sphere with the Earth's equatorial radius. Because of the inclusion of such effects as the inertial and Coriolis forces, the gravimetric factor is no longer the combination of potential and displacement Love numbers, but an independent ratio, defined as the ratio of changes in gravity on the ellipsoid, to the direct attraction at the same point. Both quantities are evaluated along the normal to the ellipsoid, as a good approximation to the local vertical. Wahr (1981a) used the radius vector instead, producing a much larger apparent latitude effect.

The standard expression for the gravimetric factor is given by Dehant *et al.* (1999):

$$\delta(\theta) = \delta_0 + \delta_+ \frac{Y^m_{n+2}}{Y^m_n} + \delta_- \frac{Y^m_{n-2}}{Y^m_n} \qquad [20]$$

By the definition of the Y^m_n's, $\delta_- = 0$ except for $m \leq n-2$, so for the $n=2$ tides we have for the diurnal tides

$$\delta(\theta) = \delta_0 + \delta_+ \frac{\sqrt{3}}{2\sqrt{2}}\left(7\cos^2\theta - 3\right)$$

and for the semidiurnal tides

$$\delta(\theta) = \delta_0 + \delta_+ \frac{\sqrt{3}}{2}\left(7\cos^2\theta - 1\right)$$

The expression for the induced potential (Wahr, 1981a) is similar, namely that the potential is gotten by replacing the term $Y_{nm}(\theta, \phi)$ in eqn [7] with

$$k_0\left(\frac{a_e}{r}\right)^{n+1} Y_{nm}(\theta, \phi) + k_+\left(\frac{a_e}{r}\right)^{n+3} Y^m_{n+2}(\theta, \phi) \qquad [21]$$

which of course recovers the conventional Love number for $k_+ = 0$.

The expressions for displacements are more complicated, partly because this is a vector quantity, but also because the horizontal displacements include spheroidal–toroidal coupling, which affects neither the vertical, the potential, nor gravity. For the degree-2 tides, the effect of coupling to the degree-4 deformation is allowed for by defining

$$\begin{aligned} h(\theta) &= h^{(0)} + \frac{1}{2}h^{(2)}\left(3\cos^2\theta - 1\right), \\ l(\theta) &= l^{(0)} + \frac{1}{2}l^{(2)}\left(3\cos^2\theta - 1\right) \end{aligned} \qquad [22]$$

Then to get the vertical displacement, replace the term $Y_{nm}(\theta, \phi)$ in eqn [7] with

$$h(\theta)\, Y^m_2(\theta, \phi) + \frac{\delta_{m0} h^P}{N^0_2} \qquad [23]$$

where the δ_{m0} is the Kronecker delta, since h^P (usually called h' in the literature) only applies for $m=0$; the N^0_2 factor arises from the way in which h^P was defined by Mathews *et al.* (1995b) .

The displacement in the $\hat{\theta}$ (North) direction is gotten by replacing the term $Y_{nm}(\theta, \phi)$ in eqn [7] with

$$l(\theta)\frac{\partial Y^m_2(\theta, \phi)}{\partial\theta} - \frac{m l^1 \cos\theta}{\sin\theta} Y^m_2(\theta, \phi) + \frac{\delta_{m1} l^P}{N^1_2} e^{i\phi} \qquad [24]$$

where again the l^P (usually called l') applies only for the particular value of $m=1$, for which it applies a correction such that there is no net rotation of the Earth. Finally, to get the displacement in the $\hat{\phi}$ (East) direction, we replace the $Y_{nm}(\theta, \phi)$ term in [7] with

$$i\left[\frac{m l(\theta)}{\sin\theta} Y^m_2(\theta, \phi) + l^1 \cos\theta \frac{\partial Y^m_2(\theta, \phi)}{\partial\theta} + \frac{\delta_{m0} \sin\theta\, l^P}{N^0_2}\right] \qquad [25]$$

where again the l^P term applies, for $m=0$, a no-net-rotation correction. The multiplication by i means that when this is applied to [7] and the real part taken, the time dependence will be $b^m_n(t)\cos m\phi - a^m_n(t)\sin m\phi$ instead of $a^m_n(t)\cos m\phi + b^m_n(t)\sin m\phi$.

Table 6 gives the generalized Love numbers for selected tides, including ellipticity, rotation, the NDFW, and anelasticity (which we discuss below). The values for the diurnal tides are from exact computations rather than the resonance approximations

Table 6 Love numbers for an Earth that includes ellipticity, rotation, anelasticity, and the NDFW resonance

	Ssa	Mf	O_1	P_1	K_1	ψ_1	M_2	M_3
δ_0	1.15884	1.15767	1.15424	1.14915	1.13489	1.26977	1.16172	1.07338
δ_+	0.00013	0.00013	0.00008	−0.00010	−0.00057	0.00388	0.00010	0.00006
δ_-	−0.00119	−0.00118						
$\Re\,[k^{(0)}]$	0.3059	0.3017	0.2975	0.2869	0.2575	0.5262	0.3010	0.093
$\Im\,[k^{(0)}]$	−0.0032	−0.0021	−0.0014	−0.0007	0.0012	0.0021	−0.0013	
k^+	−0.0009	−0.0009	−0.0008	−0.0008	−0.0007	−0.0011	−0.0006	
$\Re\,[b^{(0)}]$	0.6182	0.6109	0.6028	0.5817	0.5236	1.0569	0.6078	0.2920
$\Im\,[b^{(0)}]$	−0.0054	−0.0037	−0.0006	−0.0006	−0.0006	−0.0020	−0.0022	
$\Re\,[l^{(0)}]$	0.0886	0.0864	0.0846	0.0853	0.0870	0.0710	0.0847	0.0015
$\Im\,[l^{(0)}]$	−0.0016	−0.0011	−0.0006	−0.0006	−0.0007	−0.0001	−0.0006	
$h^{(2)}$	−0.0006	−0.0006	−0.0006	−0.0006	−0.0007	−0.0001	−0.0006	
$l^{(2)}$	0.0002	0.0002	0.0002	0.0002	0.0002	0.0002	0.0002	
$l^{(1)}$			0.0012	0.0012	0.0011	0.0019	0.0024	
l^P			–0.0002	–0.0002	–0.0003	–0.0001		

Values for the gravimetric factors are from Dehant *et al*. (1999) and for the other Love numbers from the IERS standards (McCarthy and Pétit, 2004).

given above. It is evident that the latitude dependence ranges from small to extremely small, the latter applying to the gravimetric factor, which varies by only 4×10^{-4} from the equator to 60° N. For the displacements, Mathews *et al.* (1997) show that the various coupling effects are at most 1 mm; the latitude dependence of $h(\theta)$ changes the predicted displacements by 0.4 mm out of 300.

3.06.3.2.3 Anelastic effects

All modifications to the Love numbers discussed so far apply to an Earth model that is perfectly elastic. However, the materials of the real Earth are slightly dissipative (anelastic), with a finite Q. Measurements of the Q of Earth tides were long of interest because of their possible relevance to the problem of tidal evolution of the Earth–Moon system (Cartwright, 1999); though it is now clear that almost all of the dissipation of tidal energy occurs in the oceans (Ray *et al*., 2001), anelastic effects on tides remain of interest because tidal data (along with the Chandler wobble) provide the only information on Q at frequencies below about 10^{-3} Hz.

Over the seismic band (approximately 10^{-3} to 1 Hz), Q appears to be approximately independent of frequency. A general model for frequency dependence is

$$Q = Q_0 \left(\frac{f}{f_0}\right)^{\alpha} \qquad [26]$$

where f_0 and Q_0 are reference values. In general, in a dissipative material the elastic modulus μ will in general also be a function of frequency, with $\mu(f)$ and $Q(f)$ connected by the Kramers–Kronig relation (Dahlen and Tromp, 1998, chapter 6). (We use μ because this usually denotes the shear modulus; in pure compression Q is very high and the Earth can be treated as elastic.) This frequency dependence is usually termed 'anelastic dispersion'. For the frequency dependence of Q given by [26], and α small, the modulus varies as

$$\mu(f) = \mu_0 \left[1 + \frac{1}{Q_0}\left\{\frac{2}{\alpha\pi}\left[1 - \left(\frac{f_0}{f}\right)^{\alpha}\right] + i\left(\frac{f_0}{f}\right)^{\alpha}\right\}\right] \qquad [27]$$

so there is a slight variation in the modulus with frequency, and the modulus becomes complex, introducing a phase lag into its response to sinusoidal forcing. In the limit as α approaches zero (constant Q), the real part has a logarithmic frequency dependence. Including a power-law variation [26] at frequencies below a constant-Q seismic band, the frequency dependence becomes

$$\begin{aligned}
\mu(f) &= \mu_0 \left[1 + \frac{1}{Q_0}\left\{\frac{2}{\pi}\ln\left(\frac{f_0}{f}\right)^{\alpha} + i\right\}\right], \quad f > f_m \\
\mu(f) &= \mu_0 \left[1 + \frac{1}{Q_0}\left\{\frac{2}{\alpha\pi}\left[\alpha\ln\left(\frac{f_m}{f_0}\right) + 1 - \left(\frac{f_m}{f}\right)^{\alpha}\right] + i\left(\frac{f_m}{f}\right)^{\alpha}\right\}\right], \quad f < f_m
\end{aligned} \qquad [28]$$

where f_m is the frequency of transition between the two Q models.

Adding anelasticity to an Earth model has three effects on the computed Love numbers:

1. Anelastic dispersion means that the elastic constants of an Earth model found from seismology must be adjusted slightly to be appropriate for tidal frequencies. As an example, Dehant *et al.* (1999) find that for an elastic Earth model the gravimetric factor δ_0 is 1.16030 for the M_2 tide; an anelastic model gives 1.16172; for $h^{(0)}$ the corresponding values are 0.60175 and 0.61042.
2. Dispersion also means that the Love numbers vary within the tidal bands. For the semidiurnal and diurnal tides, the effect is small, especially compared to the NDFW resonance; in the long-period bands, it is significant as f approaches zero. The usual formulation for this (McCarthy and Pétit, 2004) is based on a slightly different form of [28], from Smith and Dahlen (1981) and Wahr and Bergen (1986) ; the Love numbers vary in the long-period band as

$$L(f) = A - B\left\{\cot\frac{\alpha\pi}{2}\left[1-\left(\frac{f_m}{f}\right)^{\alpha}\right]+\mathrm{i}\left(\frac{f_m}{f}\right)^{\alpha}\right\} \quad [29]$$

where A and B are constants for each Love number. For the IERS standards, $\alpha = 0.15$ and $f_m = 432$ cpd (a period of 200 s). A and B are 0.29525 and -5.796×10^{-4} for k^0, 0.5998 and -9.96×10^{-4} for $h^{(0)}$, and 0.0831 and -3.01×10^{-4} for $l^{(0)}$.
3. As eqn [29] shows, the Love numbers also become complex-valued, introducing small phase lags into the tides. There are additional causes for this; in particular, the NDFW frequency can have a small imaginary part because of dissipative core–mantle coupling, and this will produce complex-valued Love numbers even in an elastic Earth. Complex-valued Love numbers can be used in extensions of eqns [7] and [8]; for example if the elastic Love-number combination introduces no phase shift (as for gravity) itself in phase, the real part is multiplied by $[a_n^m(t)\cos m\phi + b_n^m(t)\sin m\phi]$ and the imaginary part by $[b_n^m(t)\cos m\phi - a_n^m(t)\sin m\phi]$.

The most recent examination of tidal data for anelastic effects (Benjamin *et al.*, 2006) combined data from diurnal tides (in the potential, as measured by satellites), the Chandler wobble, and the 19-year nodal tide. They find a good fit for α between 0.2 and 0.3, with $f_m = 26.7$ cpd; using the IERS value of f_m gave a better fit for α between 0.15 and 0.25.

3.06.4 Tidal Loading

A major barrier to using Earth tides to find out about the solid Earth is that they contain signals caused by the ocean tides – which may be signal or noise depending on what is being studied. The redistribution of mass in the ocean tides would cause signals even on a rigid Earth, from the attraction of the water; on the real Earth they also cause the Earth to distort, which causes additional changes. These induced signals are called the 'load tides', which combine with the body tide to make up the total tide (**Figure 1**).

3.06.4.1 Computing Loads I: Spherical Harmonic Sums

To compute the load, we start with a description of the ocean tides, almost always as a complex-valued function $H(\theta', \phi')$, giving the amplitude and phase of a particular constituent over the ocean; we discuss such ocean-tide models in more detail in Section 3.06.4.3. The loads can then be computed in two ways: using a sum of spherical harmonics, or as a convolution of the tide height with a Green function.

In the first approach, we expand the tidal elevation in spherical harmonics:

$$H(\theta', \phi') = \sum_{n=0}^{\infty}\sum_{m=-n}^{n} H_{nm}Y_{nm}(\theta', \phi') \quad [30]$$

where the Y_{nm} are as in the section on tidal forcing, and the H_{nm} would be found from

$$\begin{aligned} H_{nm} &= \int_0^{\pi}\sin\theta'\,\mathrm{d}\theta'\int_0^{2\pi}\mathrm{d}\phi H(\theta', \phi')\,Y_{nm}^{*} \\ &\equiv \int_{\Omega} H(\theta', \phi')\,Y_{nm}^{*}\,\mathrm{d}\Omega \end{aligned} \quad [31]$$

where we use Ω for the surface of the sphere. Note that there will be significant high-order spherical-harmonic terms in H_{nm}, if only because the tidal height goes to zero over land: any function with a step behavior will decay only gradually with increasing degree.

The mass distribution H causes a gravitational potential on the surface of the Earth, which we call V^{L}. This potential is given by the integral over the surface of the potential function times H; the potential function is proportional to r^{-1}, where r is the linear distance from the location (θ, ϕ) to the mass at (θ', ϕ'), making the integral

$$V^{\mathrm{L}}(\theta, \phi) = G\rho_{\mathrm{w}}a^2\int_{\Omega}\frac{H(\theta', \phi')}{r}\,\mathrm{d}\Omega \quad [32]$$

where ρ_w is the density of seawater, and G and a are as in Section 3.06.2.1. We can write the r^{-1} in terms of angular distance Δ:

$$\frac{1}{r} = \frac{1}{2a\sin(\Delta/2)} = \frac{1}{a}\sum_{n=0}^{\infty} P_n(\cos\Delta) = \frac{1}{a}\sum_{n=0}^{\infty}\sum_{m=-n}^{n}\frac{4\pi}{2n+1}Y_{nm}(\theta',\phi')\,Y_{nm}^{*}(\theta,\phi) \qquad [33]$$

where we have again used the addition theorem [5]. Combining the last expression in [33] with the spherical harmonic expansion [30] and the expression for the potential [32] gives the potential in terms of spherical harmonics:

$$V^{L} = G\rho_w a\sum_{n=0}^{\infty}\sum_{m=-n}^{n}\frac{4\pi}{2n+1}H_{nm}Y_{nm}(\theta,\phi) \qquad [34]$$

We have found the potential produced by the load because this potential is used, like the tidal potential, in the specification of the Earth's response to the load. Specifically, we define the load Love numbers k'_n, h'_n, and l'_n such that, for a potential V^L of degree n, we have

$$u_n^z = h'_n\frac{V_n^L}{g}, \quad u_n^b = l'_n\frac{\nabla_1 V_n^L}{g}, \quad V_n = k'_n V_n^L \qquad [35]$$

where u_n^z is the vertical displacement (also of degree n), u_n^b is the horizontal displacement, and V_n is the additional potential produced by the deformation of the Earth. These load Love numbers, like the Love numbers for the tidal potential, are found by integrating the differential equations for the deformation of the Earth, but with a different boundary condition at the surface: a normal stress from the load, rather than zero stress. For a spherical Earth, these load numbers depend only on the degree n of the spherical harmonic.

To compute the loads, we combine the definition of the load Love numbers [35] with the expression [34], using whichever combination is appropriate for some observable. For example, for vertical displacement u^z this procedure gives

$$u^z(\theta,\phi) = \frac{G\rho_w a}{g}\sum_{n=0}^{\infty}\sum_{m=-n}^{n}\frac{4\pi}{2n+1}h'_n H_{nm}Y_{nm}(\theta,\phi) = \frac{\rho_w}{\rho_E}\sum_{n=0}^{\infty}\sum_{m=-n}^{n}\frac{3h'_n}{2n+1}H_{nm}Y_{nm}(\theta,\phi) \qquad [36]$$

where ρ_E is the mean density of the Earth. A similar expression applies for the induced potential, with k'_n replacing h'_n; for the effective tide-raising potential, sometimes called the 'self-attraction loading' or SAL (Ray, 1998), we would use $1 + k'_n - h'_n$.

Many terms are needed for a sum in [36] to converge, but such a sum provides the response over the whole Earth. Ray and Sanchez (1989) used this method to compute radial displacement over the whole Earth, with $n = 256$, and special methods to speed the computation of the H_{nm} coefficients in eqn [31]. In any method that sums harmonics, there is always room for concern about the effects of Gibbs' phenomenon (Hewitt and Hewitt, 1979) near discontinuities, but no such effect was observed in the displacements computed near coastlines. Mitrovica *et al.* (1994) independently developed the same method, extended it to the more complicated case of horizontal displacements, and were able to make calculations with $n = 2048$.

Given a global ocean-tide model and a need to find loads over the entire surface, this summation technique requires much less computation than the convolution methods to be discussed in the next section. For gravity the contributions from the Earth's response are, from eqn [16], $-(n+1)k'_n V_n^L/a$ from the induced potential and $2h'_n V_n^L/a$ from the displacement, making the sum

$$\delta g(\theta,\phi) = \frac{3g\rho_w}{a\rho_E}\sum_{n=0}^{\infty}\sum_{m=-n}^{n}\frac{2h'_n-(n+1)k'_n}{2n+1}H_{nm}Y_{nm}(\theta,\phi) \qquad [37]$$

While this sum might appear to converge more slowly than eqn [36] because of the $n+1$ multiplying k'_n, the convergence is similar because for large n, nk'_n approaches a constant value, which we term k'_∞. All three load Love numbers have such asymptotic limits for large n:

$$\text{As } n \Rightarrow \infty \;\; h'_n \Rightarrow h'_\infty \;\; nk'_n \Rightarrow k'_\infty \;\; nl'_n \Rightarrow l'_\infty \qquad [38]$$

so that the sum [37] converges reasonably well. A similar sum can be used to get the gravity from the direct attraction of the water:

$$\frac{3g\rho_w}{a\rho_E}\sum_{n=0}^{\infty}\sum_{m=-n}^{n}\frac{1}{4n+2}H_{nm}Y_{nm}(\theta,\phi)$$

(Merriam, 1980; Agnew, 1983).

However, summation over harmonics is not well suited to quantities that involve spatial derivatives, such as tilt or strain. To find the load tides for these, we need instead to employ convolution methods, which we now turn to.

3.06.4.2 Computing Loads II: Integration Using Green Functions

If we only want the loads at a few places, the most efficient approach is to multiply the tide model by a Green function which gives the response to a point load, and integrate over the area that is loaded by the tides. That is, we work in the spatial domain rather than, as in the previous section, in the wave number domain; there is a strict analogy with Fourier theory, in which convolution of two functions is the same as multiplying their Fourier transforms. Convolution methods have other advantages, such as the ability to combine different ocean-tide models easily, include more detail close to the point of observation, and handle any of the Earth-tide observables. The standard reference on the procedure remains the classic paper of Farrell (1972); Jentzsch (1997) is a more recent summary.

More formally, we find the integral over the sphere (in practice over the oceans)

$$\int_0^{\pi} r \sin\theta' \mathrm{d}\theta' \int_0^{2\pi} r \,\mathrm{d}\phi' G_{\mathrm{L}}(\theta, \phi, \theta', \phi') \rho_{\mathrm{w}} H(\theta', \phi') \quad [39]$$

where G_{L} is the Green function for an effect (of whatever type) at (θ, ϕ) from a point mass (δ-function) at (θ', ϕ'); $\rho_{\mathrm{w}} g H r^2 \sin\theta \,\mathrm{d}\theta \,\mathrm{d}\phi$ is the applied force.

The Green functions are found, not directly, but by forming sums of combinations of the load Love numbers. The first step is to find the potential from a point mass. Take $H = \rho_{\mathrm{w}} a^2 \delta(\theta', \phi')$, (where δ is the Dirac delta-function). Substitute this into eqn [32], using the sum in $P_n(\cos\Delta)$ in eqn [33]. This gives the potential as

$$\begin{aligned} V^{\mathrm{L}}(\theta, \phi) &= G\rho_{\mathrm{w}} a \int_{\Omega} H(\theta', \phi') \sum_{n=0}^{\infty} P_n(\cos\Delta) \mathrm{d}\Omega \\ &= \frac{ga}{M_{\mathrm{E}}} \sum_{n=0}^{\infty} P_n(\cos\Delta) \end{aligned} \quad [40]$$

which shows that the degree-n part of the potential is $V_n^{\mathrm{L}} = ga/M_E$, independent of n. So, to compute vertical displacement we would apply this potential to the load Love number h'_n, getting the displacement

$$u^z = \frac{a}{M_{\mathrm{E}}} \sum_{n=0}^{\infty} h'_n \frac{V_n^{\mathrm{L}}}{g} = \frac{a}{M_{\mathrm{E}}} \sum_{n=0}^{\infty} h'_n P_n(\cos\Delta) = G_z(\Delta) \quad [41]$$

which is thus the loading Green function for vertical displacement. Some insight into the behavior of this function can be gotten by using the asymptotic value of h'_n to write

$$\begin{aligned} G_z(\Delta) &= \frac{a}{M_{\mathrm{E}}} \sum_{n=0}^{\infty} h'_{\infty} P_n(\cos\Delta) \\ &\quad + \frac{a}{M_{\mathrm{E}}} \sum_{n=0}^{\infty} (h'_n - h'_{\infty}) P_n(\cos\Delta) \\ &= \frac{a h'_{\infty}}{2M_{\mathrm{E}} \sin\Delta/2} + \frac{a}{M_{\mathrm{E}}} \sum_{n=0}^{\infty} (h'_n - h'_{\infty}) P_n(\cos\Delta) \end{aligned} \quad [42]$$

where we have made use of [33]. The new sum will converge much more rapidly; in practice, it needs to include only enough terms for h'_n to have approached h'_{∞} to adequate precision. For Δ small, the sum approaches zero, so the analytic part shows that, for loads nearby, G_z varies as Δ^{-1}. This is the vertical displacement seen for a point load on an elastic half-space, in what is called the Boussinesq solution; in the limit of short distance, the loading problem reduces to this, which provides a useful ckeck on numerical computations.

For the horizontal displacement the Green function is

$$u^b = \frac{ga}{M_{\mathrm{E}}} \sum_{n=0}^{\infty} \frac{l'_n}{g} \frac{\partial V_n^{\mathrm{L}}}{\partial\Delta} = \frac{a}{M_{\mathrm{E}}} \sum_{n=0}^{\infty} l'_n \frac{\partial P_n(\cos\Delta)}{\partial\Delta} = G_b(\Delta) \quad [43]$$

which may again have the asymptotic part nl'_n removed and replaced by an analytic expression

$$\begin{aligned} G_b(\Delta) &= \frac{al'_{\infty}}{M_{\mathrm{E}}} \sum_{n=0}^{\infty} \frac{1}{n} \frac{\partial P_n(\cos\Delta)}{\partial\Delta} \\ &\quad + \frac{a}{M_{\mathrm{E}}} \sum_{n=0}^{\infty} (l'_n - l'_{\infty}) \frac{\partial P_n(\cos\Delta)}{\partial\Delta} \\ &= -\frac{al'_{\infty}}{M_{\mathrm{E}}} \frac{\cos(\Delta/2)[1 + 2\sin\Delta/2]}{2\sin(\Delta/2)[1 + \sin\Delta/2]} \\ &\quad + \frac{a}{M_{\mathrm{E}}} \sum_{n=0}^{\infty} (nl'_n - l'_{\infty}) \frac{1}{n} \frac{\partial P_n(\cos\Delta)}{\partial\Delta} \end{aligned} \quad [44]$$

which shows the same dependence on Δ for small distances.

For gravity, there are two parts to the loading: the direct attraction of the water mass (often called the Newtonian part), and the change caused by elastic deformation of the Earth. The first part can be found analytically by using the inverse square law and computing the vertical part of the attraction. If the elevation of our point of observation is εa, with ε small, this Green function is

$$G_{gn}(\Delta) = -\frac{g}{M_{\mathrm{E}}} \left[\frac{\varepsilon + 2\sin^2\Delta/2}{(4(1+\varepsilon)\sin^2\Delta/2 + \varepsilon^2)^3/2} \right] \quad [45]$$

The elastic part of the Green function follows from the harmonic expression [37]:

$$\begin{aligned} G_{ge} &= \frac{g}{M_E}\sum_{n=0}^{\infty}(2h'_n-(n+1)k'_n)P_n(\cos\Delta) \\ &= \frac{g(2h'_\infty-k'_\infty)}{2M_E\sin\Delta/2}+\frac{a}{M_E}\sum_{n=0}^{\infty}(2(h'_n-h'_\infty) \\ &\quad -((n+1)k'_n-k'_\infty))P_n(\cos\Delta) \end{aligned} \quad [46]$$

which shows, again, a Δ^{-1} singularity for Δ small.

Likewise, the Green function for the tide-raising potential makes use of the combination $1-k'_n+h'_n$:

$$\begin{aligned} G_{\text{pot}} &= \frac{a}{M_E}\sum_{n=0}^{\infty}(1+k'_n-h'_n)P_n(\cos\Delta) \\ &= \frac{a(1-h'_\infty)}{2M_E\sin\Delta/2}+\sum_{n=0}^{\infty}(k'_n-(h'_n-h'_\infty))P_n(\cos\Delta) \end{aligned} \quad [47]$$

and the Green function for tilt uses the same combination of Love numbers, but with the derivative of the P_n's:

$$\begin{aligned} G_t &= \frac{-1}{M_E}\sum_{n=0}^{\infty}(1+k'_n-h'_n)\frac{\partial P_n(\cos\Delta)}{\partial\Delta} \\ &= \frac{(1-h'_\infty)\cos(\Delta/2)}{4M_E\sin^2\Delta/2}-\sum_{n=0}^{\infty}(k'_n-(h'_n-h'_\infty))\frac{\partial P_n(\cos\Delta)}{\partial\Delta} \end{aligned} \quad [48]$$

which has a Δ^{-2} singularity for Δ small. The tilt is thus much more sensitive to local loads than the other observables we have so far discussed.

The remaining Green function is that for strain, specifically for the strain in the direction of the load

$$e_{\Delta\Delta} = \frac{1}{a}\frac{\partial u^b}{\partial\Delta}+\frac{u^z}{a}$$

from which the Green function is, from [41] and [43],

$$\begin{aligned} G_{\Delta\Delta} &= \frac{1}{M_E}\sum_{n=0}^{\infty}h'_nP_n(\cos\Delta)+\frac{1}{M_E}\sum_{n=0}^{\infty}l'_n\frac{\partial^2P_n(\cos\Delta)}{\partial\Delta^2} \\ &= \frac{h'_\infty}{2M_E\sin\Delta/2}+\frac{1}{M_E}\sum_{n=0}^{\infty}(h'_n-h'_\infty)P_n(\cos\Delta) \\ &\quad +\frac{l'_\infty}{M_E}\sum_{n=0}^{\infty}\frac{1}{n}\frac{\partial^2P_n(\cos\Delta)}{\partial\Delta^2}+\frac{1}{M_E}\sum_{n=0}^{\infty}(l'_n-l'_\infty) \\ &\quad \times\frac{\partial^2P_n(\cos\Delta)}{\partial\Delta^2} \\ &= \frac{h'_\infty}{2M_E\sin\Delta/2}+\frac{1}{M_E}\sum_{n=0}^{\infty}(h'_n-h'_\infty)P_n(\cos\Delta) \\ &\quad +\frac{l'_\infty}{M_E}\frac{1+\sin\Delta/2+\sin^2\Delta/2}{4\sin^2\Delta/2[1+\sin\Delta/2]} \\ &\quad +\frac{1}{M_E}\sum_{n=0}^{\infty}(l'_n-l'_\infty)\frac{\partial^2P_n(\cos\Delta)}{\partial\Delta^2} \end{aligned} \quad [49]$$

which again shows a near-field singularity of Δ^{-2}. This behavior also holds for the strain perpendicular to the direction to the load; since this is given by

$$\frac{u^z}{a}+\frac{\cos\Delta}{\sin\Delta}\frac{u^b}{a} \quad [50]$$

there is no need to compute a separate Green function for it. The Green function for linear strain that would be used in [39] is

$$\begin{aligned} G_L(\Delta,\zeta) &= G_{\Delta\Delta}(\Delta)\cos^2\zeta \\ &\quad +\left[\frac{G_z(\Delta)}{a}+\cot\Delta\frac{G_b(\Delta)}{a}\right]\sin^2\zeta \end{aligned} \quad [51]$$

where ζ is the azimuth of the load relative to the direction of extension. Areal strain has a complicated dependence on distance, because it is zero for a point load on a halfspace, except right at the load.

All of the Green functions are computed by finding the load Love numbers for a range of n, and forming the various sums. Farrell (1972) formed the sums up to $n=10\,000$; the Love numbers can be computed at values of n spaced logarithmically and interpolated to intermediate values. Several numerical methods to accelerate the convergence of the sums are described by Farrell (1972) and Francis and Dehant (1987). The Green functions tabulated by Farrell (1972) (with the addition of the potential function by Farrell (1973)) are still widely used; Jentzsch (1997) tabulates a set for the PREM model. Kamigaichi (1998) has discussed the variations in the strain and tilt Green functions at shallow depths, forming sums up to $n=4\times10^6$; the results show a smooth transition between the surface functions given here, and the Boussinesq results for the response of a halfspace at depth. Such burial does however eliminate the singularity in the strain Green functions. Examinations of the extent to which local structure, particularly lateral variations, affects computed load tides, have not be plentiful – perhaps mostly because the data most sensitive to such effects, strain and tilt, are affected by other local distortions (Section 3.06.6.1). As with the Love numbers for the body tides, the load Love numbers will be affected by rotation, ellipticity, anisotropy, and anelasticity. The first two produce, again, a resonant response from the NDFW, though only for loads of degree 2 and order 1 (Wahr and Sasao, 1981); Pagiatakis (1990) has examined effects from the others.

It is also possible to define load Love numbers, and Green functions derived for them, for transverse rather than normal stress, to describe the deformation of the Earth by wind stress or ocean currents, including tidal currents; see Merriam (1985, 1986) and Wilhelm (1986).

3.06.4.3 Ocean Tide Models

Of course, to compute loads, we need a description of the ocean tides. Producing such models globally is a difficult task that has been pursued for some time (Cartwright, 1977, 1999). The intractability of the relevant equations, the complexity of the geometry, and the sensitivity of the results to details in the models long precluded numerical solutions, one difficulty being that the oceans have barotropic modes of oscillation with periods close to the diurnal and semidiurnal tidal bands. At the same time, it was very difficult to measure tides in deep water. All this meant that until recently there were no good tidal models for computing loads.

From the Earth-tide standpoint what is important is that increasing computational power has finally rendered numerical solutions possible for realistic geometries, and that satellite altimetry has provided data with global coverage (Le Provost *et al.*, 1995, 1998; Andersen *et al.*, 1995; Shum *et al.*, 1997; Desai *et al.*, 1997). The ocean models now available are often adequate to produce estimated loads that are as accurate as available Earth-tide measurements.

Perhaps the biggest difficulty in modeling the tides is the need to represent the bathymetry in adequate detail in the model, especially in shallow water, where the wavelengths are short. This need, and the relatively coarse spacing of the altimetry data, has meant that tidal models are still divided into two groups: global and local. Global models are computed on a relatively coarse mesh (say 0.5°), and rely heavily on altimetry data (e.g., Egbert and Erofeeva, 2002); they often cannot adequately model the resonances that occur in some bodies of water (such as the Bay of Fundy), for which local models are required: these use a finer mesh, and often rely more on local tide-gauge data. Obviously, a local model is not important for computing loads unless the data are collected close by.

Most tidal models are given for particular tidal constituents, usually at least one diurnal and one semidiurnal. Unless a local resonance is present, the loads for other harmonics can be found by scaling using the ratios of the amplitudes in the equilibrium tide (Le Provost *et al.*, 1991).

3.06.4.4 Computational Methods

Essentially all load programs perform the convolution [39] directly, either over the grid of ocean cells (perhaps more finely divided near the load) or over a radial grid. Two that are generally available are GOTIC (Matsumoto *et al.*, 2001) and SPOTL (Agnew, 1996). Bos and Baker (2005) have recently compared the results from four programs, albeit only for gravity, which is least sensitive to local loads. They found variations of a few percent because of different computational assumptions, and different coastline models. Most global ocean-tide models do not represent coastlines more accurately than their rather coarse mesh size, so some local refinement is needed. Fortunately, this problem has essentially been solved by the global coastal representations made available by Wessel and Smith (1996) – except in the Antarctic, where their coastline is (in places) the ice shelves, beneath which the tides are still present.

Figure 8 shows the computed loads for a region (Northwest Europe) with large and complex local tides. The vertical displacement and gravity loads have roughly similar forms, but the tilt and linear strain have a very different pattern, being much more concentrated near the coast, as might be expected from the different near-field behavior of their Green functions.

3.06.5 Analyzing and Predicting Earth Tides

As noted in Section 3.06.1, the tidal forces can be described to extremely high precision and accuracy, and the body tides and tidal loading can often be modeled to an accuracy that exceeds that of tidal measurements. Such measurements do however provide a check on these models, and in some cases allow them to be improved, so we briefly describe how tidal parameters are extracted from the data, and how the data are obtained. This is important whether we aim to measure the tides, use modeled tides as a calibration signal, or predict the tides to high accuracy to check the quality of ongoing measurements.

3.06.5.1 Tidal Analysis and Prediction

As noted in Section 3.06.1, the analysis of time series for tidal response is just a special case of finding the transfer function, or admittance, of a linear system, a concept first introduced into tidal analysis by Munk and Cartwright (1966) . Because the tides are very band-limited, we can find the 'tidal admittance', $W_T(f)$, only for frequencies at which $X_T(f)$ contains significant energy. For ocean tides it is most

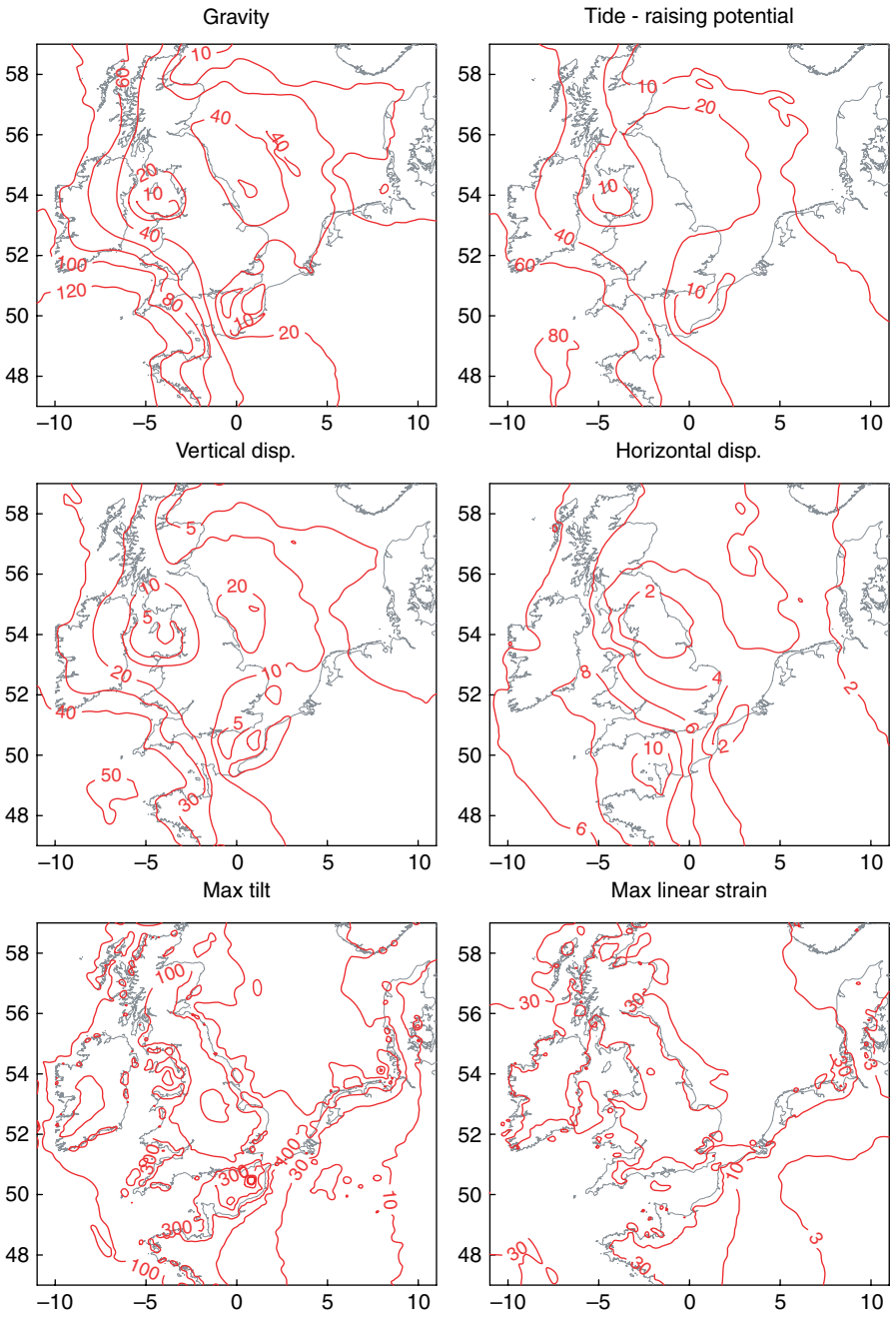

Figure 8 Loads for the M_2 tide, computed by the Green function method for the TPXO6.2 tidal model of Egbert and Erofeeva (2002), combined with a detailed model of the North Sea tides by the same group. Only the amplitude of the complex-valued quantities is shown; for tilt, displacement, and strain the value is taken along the azimuth that maximizes the amplitude. The units are nm s^{-2} for gravity, mm for the potential height and the displacements, and 10^{-9} for tilt and strain; for clarity the contour interval is logarithmic for the last two.

meaningful to take $x_T(t)$ to be the local value of the tide-raising potential, or for some analyses the tide computed for a nearby site (Cartwright *et al.*, 1969). In Earth-tide studies it may be more convenient to take as reference the tides expected for an oceanless, but otherwise realistic, earth model, so that any departure of $W(f)$ from unity will then reflect the effect of ocean loads or the inadequacy of the model.

The theory described in Section 3.06.3.2 shows that, except for the NDFW resonance, $W(f)$ for an oceanless Earth varies only very slightly with frequency. The ocean tides show more variability, but only in limited areas do they have resonances within the tidal bands, so that in general the ocean load also varies smoothly with frequency (Garrett and Munk, 1971). Even the local resonances in certain bays and gulfs have a low enough Q that the response is smoothly varying over (say) the entire semidiurnal band (Ku *et al.*, 1985). So, the more closely spaced two frequencies are, the closer the corresponding values of $W(f)$ will be, an assumption Munk and Cartwright (1966) dubbed the 'credo of smoothness'.

A naive way to find the tidal response is to take the Fourier transform of the data (using a fast Fourier transform), and use the amplitudes and phases of the result. This is a poor choice for two reasons. One problem is that the frequencies computed by the usual definition of the discrete Fourier transform usually do not coincide with the frequencies of the tidal harmonics – especially if the length of the transform, N, is chosen to work well with a fast Fourier transform algorithm. In addition, any noise will bias the amplitudes of the coefficients to be larger than the true values.

If spectral analysis is to be used, a much better method is the cross-spectral technique described by Munk and Cartwright (1966) . This method has lower-frequency resolution than others to be discussed, but makes the fewest assumptions about the form of $W(f)$, and also provides estimates of the noise as a function of frequency. This is useful because many methods assume the noise to be the same at all frequencies, and it may not be; in particular, the noise is sometimes observed to rise sharply in the tidal bands, a phenomenon called 'tidal cusping' (Munk *et al.*, 1965; Ponchaut *et al.*, 2001; Colosi and Munk, 2006). The cross-spectral method does however require large amounts of data to perform reliably. The procedure is described in full by Munk and Cartwright (1966) ; it depends on finding the cross-spectrum between a noise-free reference series and the data, using a slow Fourier transform to make the Fourier frequencies match the tidal frequencies relatively well, windowing to reduce bias from spectral leakage, and averaging to get a statistically consistent estimate.

By far the commonest approach to tidal analysis is least-squares fitting of a set of sinusoids with known frequencies – chosen, of course, to match the frequencies of the largest tidal constituents. That is, we aim to minimize the sum of squares of residuals:

$$\sum_{n=0}^{N}\left[y_n - \sum_{l=1}^{L}\left(A_l\cos(2\pi f_l t_n) + B_l\sin(2\pi f_l t_n)\right)\right]^2 \qquad [52]$$

which expresses the fitting of L sine–cosine pairs with frequencies f_l to the N data y_n, the f's being fixed to the tidal harmonic frequencies and the A's and B's being solved for.

The usual assumption behind a least-squares analysis is that the residual after fitting the sinusoids will be statistically independent random variables; but this is valid only if the noise spectrum is white, which is usually not so. One departure from whiteness is the presence of increased long-period noise outside the tidal bands; this can be removed by filtering the data before analyzing it. A more difficult problem is the tidal cusping just referred to. If the noise spectrum rises to a higher level inside the tidal bands, perhaps very much higher around the frequencies of the radiational tides, this needs to be allowed for in fitting the tides, and in finding the errors in the final tidal parameters. In particular, the relative error for a harmonic of amplitude A analyzed over a total time span T is approximately $2P(f)/A^2T$, where $P(f)$ is the noise power spectral density at the frequency of that harmonic (Munk and Hasselmann, 1964; Cartwright and Amin, 1986). If excess energy in the tidal bands is not allowed for, the errors can be underestimated by significant amounts.

The main problem with using [52] directly for tidal analysis comes from the fine-scale frequency structure of the tidal forcing, particularly the nodal modulations. Leaving such variations out of [52], and only solving for a few large harmonics, will be inaccurate. But the simplest way of including nodal and other modulations, namely by including the satellite harmonics in [52], is not possible because the solution will be unstable unless we have 19 years of data. This instability is general, and applies whenever we try to solve for the amplitudes of harmonics separated in frequency by less than $1/T$, where T is the record length (Munk and Hasselmann, 1964). This problem is not restricted to the nodal modulation; for example, with only a month of data, we cannot get reliable results for the P_1 and K_1 lines, since they are separated by only 0.15 cycles/month.

All least-squares tidal analysis thus has to include assumptions about tidal harmonics closely spaced in frequency – which comes to an implicit assumption about the smoothness of the admittance. Usually, the admittance is assumed to be constant over frequency

ranges of width $1/T$ around the main constituents, summing all harmonics within each such range to form (slowly varying) sinusoidal functions to replace the sines and cosines of [52]. Of course, if we then wish to assign the resulting amplitude to a particular harmonic (say M_2), we need to correct the amplitudes found by the ratio of this sinusoidal function to the single harmonic. All this adds complexity to the existing analysis programs (Tamura *et al.*, 1991; Wenzel, 1996; Pawlowicz *et al.*, 2002; Foreman, 2004; Van Camp and Vauterin, 2005).

A quite different approach to tidal analysis is the 'response method', also introduced by Munk and Cartwright (1966) . This does not use an expansion of the tidal potential into harmonics, but rather treats it as a time series to be fit to the data, using a set of weights to express the admittance. Lambert (1974) and Merriam (2000) have applied this method to Earth tides, and it is standard in the estimation of tides from satellite altimetry.

The basic approach is to find the tides as a weighted sum over the time variations of each spherical harmonic (not harmonics in time):

$$y(t) = \sum_{n=2}^{\infty} \sum_{m=-n}^{n} \sum_{l=-L_{nm}}^{L_{nm}} w_{nl}^{m}[a_n^m(t-l\Delta)] + ib_n^m(t-l\Delta)] \quad [53]$$

where the $a_n^m(t)$ and $b_n^m(t)$ are the time-varying functions that sum to give the potential in [8]. The complex-valued weights w_{nl}^m are called 'response weights'; their Fourier transform gives the admittance $W(f)$. So, for example, a single complex weight for each n and m (i.e., setting $L_{nm} = 0$) amounts to assuming a constant W for each degree and order – though even one complex weight can express both amplitude and phase response. Including more weights, with time lags (the sum over l), allows the admittance to vary with frequency, smoothly, across each tidal band. The lag interval is usually chosen to be 2 days, which makes the admittance smooth over frequencies of greater than 0.5 cpd; note that the lags can include the potential at future times because the admittance is being fit over only a narrow frequency band.

3.06.5.1.1 Predicting tides

All tidal predictions, other than those based on the response method, use a harmonic expansion similar to eqn [11]:

$$x(t) = \sum_{k=1}^{K} A_k \cos[2\pi f_k(t-t_0) + \phi_k^0(t_0) + \phi_k] \quad [54]$$

where the A_k's and ϕ_k's are amplitudes and phases (the 'harmonic constants') for whatever is being predicted. The f_k's are the frequencies of the different harmonics, and the ϕ_k^0 's are the phases of these at a reference time t_0.

Any user of tidal constants should be aware of two pitfalls relating to the conventions for phase. One is a sign convention: whether positive phases represent lags (true in much of the older literature) or leads. The other is the reference time used. The 'local phase' is one choice, in which zero phase (for each harmonic) is at a time at which the potential from that harmonic is locally a maximum. For ocean tides this phase is usually denoted as κ (with positive phases for lags). For Earth tides local phase is convenient because on a SNREI Earth it is zero for gravity, NS tilt, vertical displacement, and areal strain. The other choice is the Greenwich phase G, in which the phase is taken to be zero (for each harmonic) at a time at which its potential would be a maximum at 0 longitude. If given for a number of places, this phase provides a 'snapshot' of the distribution of the tides at a particular instant; this phase is the norm in ocean-tide models. Since the time between maximum at Greenwich and maximum at a local place depends only on the spherical harmonic order m and on the Earth rotating 360° every 24 hs, the relationship between k and G is simple, and depends only on the tidal species number m and the longitude ϕ_W; the frequency of the harmonic is not involved. The relationship is conventionally written as

$$G = \kappa - m\phi_W$$

where for both phases a lag is taken to be positive, and longitude ϕ_W to be positive going West.

The primary complications in predicting the tides come, once again, from the various long-term modulations, notably the nodal modulations discussed in Section 3.06.2.3. Classical prediction methods, which used only a few constituents to minimize computation, applied nodal corrections to the A_k's and ϕ_k's of these few harmonics to produce new values that would be valid for (say) each year; a complication, since the corrections themselves change with time.

A more computationally intensive but conceptually simpler approach uses a large number of harmonics in the sum [54], including all satellite harmonics, thus automatically producing the modulations. The amplitudes and phases of a few harmonics are interpolated to give those of all harmonics, again on the assumption

that the admittance is smooth; for example, through a spline interpolation of the real and imaginary parts of $W(f)$ (Le Provost *et al.*, 1991).

3.06.6 Earth-Tide Instrumentation

Because the Earth tides are so small, building instruments to detect them has long been a challenge, though an easier one over time, as sensitive transducers and digital recording have become more readily available.

The earliest measurements were of tidal tilts, and over the years a wide variety of tiltmeters have been designed; Agnew (1986) describes many of them, and the designs have changed little since then. They generally fall into two classes: small instruments that sense the motion of a pendulum or of a bubble in a fluid, and larger systems that measure the motion of a fluid in a long pipe. The former are usually referred to as short-base tiltmeters, and are now generally installed in boreholes in order to obtain adequate thermal stability and relatively low rates of drift. The latter, called long-base systems, are usually installed in tunnels a few tens of meters long or longer (e.g., d'Oreye and Zürn, 2005), though a very few instruments, several hundred meters in length, have been installed near the ground surface. A similar division exists in strainmeters (Agnew, 1986): there are very short-base systems, many installed in boreholes, longer instruments installed in tunnels, and a few very long instruments, using laser light rather than physical length standards, some at the surface and others underground. One other class of instrument sensitive to tidal deformations is the ring-laser gyroscope (Schreiber *et al.*, 2003), which detects tilts that alter the orientation of the instrument relative to the Earth's spin axis.

Historically, the second type of Earth tide to be detected was changes in gravity, and many such measurements have been made with a variety of types of gravimeters (Torge, 1989). The bulk of these used metallic springs, arranged so that changes in gravity caused extension of the spring, leading to significant phase lags and hysteresis. Such measurements are however significant in showing the widespread effects of load tides (Llubes and Mazzega, 1997), and provided early evidence of the effect of the NDFW on tidal data (see, e.g., Neuberg *et al.* (1987)). These uncertain phase lags are reduced by applying feedback, which was first done in the instrument of LaCoste and Romberg (Harrison and LaCoste, 1978); this, supplied with electronic feedback, remains useful for tidal measurements. The lowest-noise tidal gravimeter is the superconducting gravimeter (Goodkind, 1999), in which a superconducting sphere is suspended in a magnetic field at liquid-helium temperatures. This gives a system with very low noise (especially at long periods) and little drift. At the periods of the semidiurnal tides, the noise ranges from −130 to −140 dB (relative to 1 $m^2 s^{-4}$), with the noise being about 5 dB higher in the diurnal band (Rosat *et al.*, 2004); these levels are about 5 dB below those of spring gravimeters (Cummins *et al.*, 1991). Because the noise is so low, small tidal signals can be measured with great precision; recent examples include the detection of loading from small nonlinear ocean tides (Merriam, 1995; Boy *et al.*, 2004) and the discrimination between the loads from equilibrium and dynamic models for the long-period ocean tides (Iwano *et al.*, 2005; Boy *et al.*, 2006a). The superconducting gravimeter also can provide accurate measurements of the NDFW resonance (Zürn *et al.*, 1986; Florsch *et al.*, 1994; Sato *et al.*, 1994, 2004). However, unlike the spring gravimeters, the superconducting instrument is not portable.

Comparing the size of the load tides in **Figure 8** with the rms body tides in **Figure 6** shows that even the largest loads are but a few percent of the total gravity tide. So, to get accurate measurements of the load tides, the gravimeter must be calibrated with extreme accuracy, at least to a part in 10^3. An even higher level of accuracy is needed if tidal gravity measurements are to discriminate between the predictions of different Earth models. Calibration to this level has proved to be difficult. One method, usable only with spring gravimeters, is to make gravity measurements over a wider range and interpolate to the small range of the tides. For superconducting gravimeters, which cannot be moved, one method is to sense the response to known moving masses (Achilli *et al.*, 1995); this is not in general possible with spring gravimeters because of their more complicated mass distribution. Another method, applicable to both types, is to place the instrument on a platform that can be moved vertically by known amounts to produce small accelerations of the same size as the tides (Richter *et al.*, 1995). The most common approach is now to operate an absolute gravimeter next to a tidal system for several days and find the scale factor by direct comparison (Hinderer *et al.*, 1991; Francis *et al.*, 1998; Tamura *et al.*, 2005). For absolute systems the scale is set by

atomic standards known to much higher accuracy than is required, and comparison tests (Francis and van Dam, 2002) confirm that this method can provide calibrations to 10^{-3}. Baker and Bos (2003) summarize tidal measurements from both spring and superconducting gravimeters; from the greater scatter for the in-phase components of the residual tide they conclude that systematic errors in the calibration remain, with errors up to 4×10^{-3} in some cases. These authors, and Boy *et al.* (2003), find too much scatter in the results to distinguish between different Earth models, or to detect any latitude dependence.

The newest procedures for measuring Earth tides are the techniques of space geodesy. Since the induced potential affects satellite orbits, modeling of these provides constraints on k_2; a particularly notable result was that of Ray *et al.* (2001), who were able to measure the phase lag of the solid-Earth component of the M_2 tide as $0.204° \pm 0.047°$. Positioning techniques such Very Long Baseline Interferometry (VLBI) and GPS are sensitive to all displacements, including tides. VLBI data have been used to observe the body tides, and now have sufficient precision to be sensitive to load tides as well (Sovers, 1994; Haas and Schuh, 1998; Petrov and Ma, 2003); the currently available series can provide the amplitudes of tidal constituents to better than 1 mm. However, VLBI data are available only at a few places, whose number is not increasing.

Continuous GPS data, in contrast, are available from many locations; and it is important that the tidal displacements of such locations be accurately modeled, since any inaccuracy (especially in the vertical) will bias GPS estimates of zenith delay and hence of water vapor (Dragert *et al.*, 2000; Dach and Dietrich, 2000); for the standard 1-day processing, unmodeled tidal displacements may produce, through aliasing, spurious long-period signals (Penna and Stewart, 2003).

Tidal motions can be found with GPS in two ways. One is to process data over short time spans (say, every 3 h) to produce a time series that can then be analyzed for tidal motions. The other is to include the complex amplitude of some of the larger tidal constituents (in all three directions) as unknowns in the GPS solution, solving for any unmodeled tides. Baker *et al.* (1995) and Hatanaka *et al.* (2001) took the first approach for two local areas, finding good agreement between observed and predicted loads. Khan and Scherneck (2003) also used this method, finding that the best approach was to estimate zenith delays over the same (hourly) time span as the displacement was found for. Schenewerk *et al.* (2001) used the second method for a global set of stations, taking data from every third day over 3 years; they found generally good agreement with predicted loads except at some high-latitude sites, probably because of using an older ocean-tide model; Allinson *et al.* (2004) applied this method to tidal loading in Britain. King (2006) compared the two methods for the GPS site at the South Pole (for which only load tides are present), using about 5 years of data. He found that the second method gave better results in the vertical; the two methods had comparable errors in the horizontal, with the precision being somewhat less than 1 mm. The K_1 and K_2 tides give poor results because their frequency is very close to the repeat time of the GPS constellation and its first harmonic. King and Padman (2005) used GPS to validate different ocean-tide models around Antarctica, with models specifically designed for this region predicting the loads better than the older global models.

3.06.6.1 Local Distortion of the Tides

King and Bilham (1973) and Baker and Lennon (1973) introduced an important concept into Earth-tide studies by suggesting that much of the scatter in measurements of tidal tilts was caused by strain tides which were coupled into tilts by the presence of a free surface – for example, the tunnel in which such instruments were often housed. This 'cavity effect' (Harrison, 1976) has indeed turned out to be important; any strain and tilt measurements not made with surface-mounted longbase instruments require that a cavity be created, and any such inhomogeneity in an elastic material will produce local deformations, which can produce rotations and strains that modify the tidal strains and tilts for an Earth with only radial variations. Other irregularities will have similar effects; for example, topography, which is to say an irregular free surface, will also create departures from what would be seen on a smooth Earth.

The way in which these departures are described is through the use of coupling matrices (Berger and Beaumont, 1976; King *et al.*, 1976). We can divide the actual displacement field in the Earth, $\mathbf{u}$, into two parts, $\mathbf{u}_0$, which is the displacement that would occur with no cavity (or other inhomogeneity), and $\delta\mathbf{u}$, the difference between this ideal and the actual displacement. We can perform the same decomposition on the strain tensor $\mathbf{E}$ and the local rotation vector $\boldsymbol{\Omega}$:

$$\mathbf{E} = \mathbf{E}_0 + \delta\mathbf{E}, \qquad \boldsymbol{\Omega} = \boldsymbol{\Omega}_0 + \delta\boldsymbol{\Omega}$$

The additional deformations $\delta\mathbf{E}$ and $\delta\boldsymbol{\Omega}$ will depend on the details of the inhomogeneity (e.g., the shape of the cavity) and on $\mathbf{E}_0$, but not on $\boldsymbol{\Omega}_0$ because it is a rigid rotation. If we suppose $\mathbf{E}_0$ to be homogeneous strain, then $\delta\mathbf{E}$ and $\delta\boldsymbol{\Omega}$ at any position are linear functions of $\mathbf{E}_0$, and can be related to it by a fourth-order strain–strain coupling tensor $\mathbf{C}_E$ and a third-order strain-rotation coupling tensor $\mathbf{C}_{\boldsymbol{\Omega}}$:

$$\delta\mathbf{E} = \mathbf{E}_E\mathbf{E}_0, \qquad \delta\boldsymbol{\Omega} = \mathbf{C}_{\boldsymbol{\Omega}}\mathbf{E}_0 \qquad [55]$$

In general, strain–tilt coupling involves both $\mathbf{C}_E$ and $\mathbf{C}_{\boldsymbol{\Omega}}$ (Agnew, 1986). Near the surface of the Earth there are only three independent components to $\mathbf{E}_0$; this fact, and the symmetries of the strain tensors, mean that both $\mathbf{C}_E$ and $\mathbf{C}_{\boldsymbol{\Omega}}$ have nine independent components.

An analytical solution for $\mathbf{C}_E$ and $\mathbf{C}_{\boldsymbol{\Omega}}$ exists for an ellipsoidal cavity (Eshelby, 1957); Harrison (1976) has described results for the case where one axis of the ellipsoid is vertical: the coupled strains and tilts are largest when measured in the direction along which the cavity is smallest, whether the external strain is in that direction or not. Strain measured along a long narrow cavity is not amplified very much. The limit of this is an infinite horizontal circular tunnel, for which the strains along the tunnel (or shear strains across it) are unaltered, but both vertical and horizontal strains are amplified, as has been observed in cross-tunnel measurements of strain tides (Itseuli *et al.*, 1975; Beavan *et al.*, 1979; Takemoto, 1981). Finite element modeling (Berger and Beaumont, 1976) shows that slight departures from circularity do not much alter the strain from wall to wall, but in a square tunnel the strains concentrate near the corners; strains along a finite tunnel are undistorted if they are measured more than one tunnel diameter away from an end. Tiltmeters mounted on tunnel walls, or placed on a ledge or near a crack, will be affected by strain-coupled tilts.

Inhomogeneities (including cavities) create distortion but do not add noise. They thus mean that precise comparison between data and models is difficult at best, with the exception of frequency-dependent effects such as the NDFW. There are analytical methods for approximating topographic effects (Meertens and Wahr, 1986), and while it is always possible to build a finite-element model of any inhomogeneity (Emter and Zürn, 1985; Sato and Harrison, 1990), not enough detail of the elastic constants is usually known to make results from such a model more than a rough guide. The measurements by Baker (1980), on a pier in the middle of a tunnel, which showed a 5% change in tilts measured 0.5 m apart, imply that such modeling has to be extremely detailed.

One possible way to reduce the importance of coupling is to arrange the geometry to minimize it. Measuring strain along a tunnel is one example; another is measuring tilt in a borehole: since a horizontal strain does not cause rotation of the side of the borehole, attaching the tiltmeter to this should eliminate the cavity effect. An array of such tiltmeters installed to use observed tides to map crustal inhomogeneities (Levine *et al.*, 1989; Meertens *et al.*, 1989) still produced widely scattered results. A subsequent test using closely spaced instruments in nominally uniform geology (Kohl and Levine, 1995) also showed significant differences between boreholes, and in one borehole even between two different positions. These results suggest that any short-base measurement of tilt may be significantly affected by local inhomogeneities, and so cannot be accurately compared with theoretical tidal models.

Sometimes the aim is to use the tides to determine the effects of the inhomogeneity, so that other signals seen can be corrected. The most notable case is borehole strainmeters, in which the instrument, hole, and grout cause the strain inside the instrument wall to be significantly different from that in the far field. A simplified model that assumes axial symmetry (Gladwin and Hart, 1985) provides two coupling coefficients, one for areal and one for shear strain. This can be checked using the tides (Hart *et al.*, 1996), which also allow estimation of a full coupling tensor, along the lines of eqn [55].

References

Achilli V, Baldi P, Casula G, Errani M, *et al.* (1995) A calibration system for superconducting gravimeters. *Bulletin Geodesique* 69: 73–80.

Agnew DC (1983) Conservation of mass in tidal loading computations. *Geophysical Journal of the Royal Astronomical Society* 72: 321–325.

Agnew DC (1986) Strainmeters and tiltmeters. *Reviews of Geophysics* 24: 579–624.

Agnew DC (1996) SPOTL: Some Programs for Ocean-Tide Loading, *SIO Reference Series 96-8*, Scripps Institution of Oceanography.

Allinson CR, Clarke PJ, Edwards SJ, *et al.* (2004) Stability of direct GPS estimates of ocean tide loading. *Geophysical Research Letters* 31(15): L15603, doi: 10.1029/2004GL020588.

Andersen OB, Woodworth PL, and Flather RA (1995) Intercomparison of recent ocean tide models. *Journal of Geophysical Research* 100: 25,261–25,282.

Baker TF (1980) Tidal tilt at Llanrwst, north Wales: Tidal loading and earth structure. *Geophysical Journal of the Royal Astronomical Society* 62: 269–290.
Baker TF (1984) Tidal deformations of the Earth. *Science Progress Oxford* 69: 197–233.
Baker TF and Bos MS (2003) Validating Earth and ocean tide models using tidal gravity measurements. *Geophysical Journal International* 152: 468–485.
Baker TF, Curtis DJ, and Dodson AH (1995) Ocean tide loading and GPS. *GPS World* 6(5): 54–59.
Baker TF and Lennon GW (1973) Tidal tilt anomalies. *Nature* 243: 75–76.
Bartels J (1957/1985) Tidal forces (English translation). In: Harrison JC (eds.) *Earth Tides*, pp. 25–63. New York: Van Nostrand Reinhold.
Beavan J, Bilham R, Emter D, and King G (1979) Observations of strain enhancement across a fissure. *Veröffentlichungen der Deutschen Geodätischen Kommission, Reihe B.* 231: 47–58.
Benjamin D, Wahr JM, Ray RD, Egbert GD, and Desai SD (2006) Constraints on mantle anelasticity from geodetic observations, and implications for the J_2 anomaly. *Geophysical Journal International* 165: 3–16, doi:10.1111/j.1365-246X.2006.02915.x.
Berger J (1975) A note on thermoelastic strains and tilts. *Journal of Geophysical Research* 80: 274–277.
Berger J and Beaumont C (1976) An analysis of tidal strain observations from the United States of America: II. the inhomogeneous tide. *Bulletin of the Seismological Society of America* 66: 1821–1846.
Bos MS and Baker TF (2005) An estimate of the errors in gravity ocean tide loading computations. *Journal of Geodesy* 79: 50–63.
Boy J-P, Llubes M, Hinderer J, and Florsch N (2003) A comparison of tidal ocean loading models using superconducting gravimeter data. *Journal of Geophysical Research* 108: ETG 6–1–6–17, doi:10.1029/2002JB002050.
Boy J-P, Llubes M, and Ray R, *et al*. (2004) Non-linear oceanic tides observed by superconducting gravimeters in Europe. *Journal of Geodynamics* 38: 391–405.
Boy J-P, Llubes M, Ray R, Hinderer J, and Florsch N (2006a) Validation of long-period oceanic tidal models with superconducting gravimeters. *Journal of Geodynamics* 41: 112–118.
Boy J-P, Ray R, and Hinderer J (2006b) Diurnal atmospheric tide and induced gravity variations. *Journal of Geodynamics* 41: 253–258.
Broucke RA, Zurn W, and Slichter LB (1972) Lunar tidal acceleration on a rigid Earth. *AGU Geophysical Monograph* 16: 319–324.
Brush SG (1996) *Nebulous Earth: The Origin of the Solar System and the Core of the Earth from Laplace to Jeffreys*. Cambridge: Cambridge University Press.
Bullesfeld F-J (1985) Ein Beitrag Zur Harmonischen Darstellung Des Gezeitenerzeugenden Potentials. *Veröffentlichungen der Deutschen Geodätischen Kommission, Reihe C.* 31: 3–103.
Cartwright D, Munk W, and Zetler B (1969) Pelagic tidal measurements: A suggested procedure for analysis. *EOS Transactions. American Geophysical Union* 50: 472–477.
Cartwright DE (1977) Oceanic tides. *Reports on Progress in Physics* 40: 665–708.
Cartwright DE (1999) *Tides: A Scientific History*. New York: Cambridge University Press.
Cartwright DE and Amin M (1986) The variances of tidal harmonics. *Deutsche Hydrographische Zeitschrift.* 39: 235–253.
Cartwright DE and Edden AC (1973) Corrected tables of tidal harmonics. *Geophysical Journal of the Royal Astronomical Society* 33: 253–264.
Cartwright DE and Tayler RJ (1971) New computations of the tide-generating potential. *Geophysical Journal of the Royal Astronomical Society* 23: 45–74.
Chapman S and Lindzen RS (1970) *Atmospheric Tides: Gravitational and Thermal*. New York: Gordon and Breach.
Colosi JA and Munk WH (2006) Tales of the venerable Honolulu tide gauge. *Journal of Physical Oceanography* 36: 967–996.
Cummins P, Wahr JM, Agnew DC, and Tamura Y (1991) Constraining core undertones using stacked IDA gravity records. *Geophysical Journal International* 106: 189–198.
Dach R and Dietrich R (2000) Influence of the ocean loading effect on GPS derived precipitable water vapor. *Geophysical Research Letters* 27: 2953–2956, doi:10.1029/1999GL010970.
Dahlen FA (1993) Effect of the Earth's ellipticity on the lunar potential. *Geophysical Journal International* 113: 250–251.
Dahlen FA and Tromp J (1998) *Theoretical Global Seismology*. Princeton, NJ: Princeton University Press.
Dehant V, Defraigne P, and Wahr JM (1999) Tides for a convective Earth. *Journal of Geophysical Research* 104: 1035–1058.
Desai SD (2002) Observing the pole tide with satellite altimetry. *Journal of Geophysical Research* 107(C11): 3186, doi:10.1029/2001JC001224.
Desai SD, Wahr JM, and Chao Y (1997) Error analysis of empirical ocean tide models estimated from Topex/Posecidon altimetry. *Journal of Geophysical Research* 102: 25,157–25,172.
Doodson AT (1921) The harmonic development of the tide generating potential. *Proceedings of the Royal Society Series A* 100: 305–329.
d'Oreye NF and Zürn W (2005) Very high resolution long-baseline water-tube tiltmeter to record small signals from Earth free oscillations up to secular tilts. *Review of Scientific Instruments* 76: 024,501.
Dragert H, James TS, and Lambert A (2000) Ocean loading corrections for continuous GPS: A case study at the Canadian coastal site Holberg. *Geophysical Research Letters* 27: 2045–2048.
Egbert GD and Erofeeva SY (2002) Efficient inverse modeling of barotropic ocean tides. *Journal of Atmospheric and Oceanic Technology* 19: 183–204.
Emter D and Zürn W (1985) Observations of local elastic effects on earth tide tilts and strains. In: Harrison JC (ed.) *Earth Tides*, pp. 309–327. New York: Van Nostrand Reinhold.
Eshelby JD (1957) The determination of the elastic field of an ellipsoidal inclusion and related problems. *Proceedings of the Royal Society Series A* 241: 376–396.
Farrell WE (1972) Deformation of the earth by surface loads. *Reviews of Geophysics* 10: 761–797.
Farrell WE (1973) Earth tides, ocean tides, and tidal loading. *Philosophical Transactions of the Royal Society Series A* 272: 253–259.
Florsch N, Chambat F, Hinderer J, and Legros H (1994) A simple method to retrieve the complex eigenfrequency of the Earth's nearly diurnal free wobble: Application to the Strasbourg superconducting gravimeter data. *Geophysical Journal International* 116: 53–63.
Foreman MGG (2004) Manual for Tidal Heights Analysis and Prediction., *Pacific Marine Science Report 77-10*. Institute of Ocean Sciences, Patricia Bay, Sidney, BC.
Francis O and Dehant V (1987) Recomputaiton of the Green's functions for tidal loading estimations. *Bulletin d'Information des Marées Terrestres* 100: 6962–6986.
Francis O and van Dam T (2002) Evaluation of the precision of using absolute gravimeters to calibrate superconducting gravimeters. *Metrologia* 39: 485–488.
Francis O, Niebauer TM, Sasagawa G, Klopping F, and Gschwind J (1998) Calibration of a superconducting

gravimeter by comparison with an absolute gravimeter FG5 in Boulder. *Geophysical Research Letters* 25: 1075–1078.
Garrett C and Munk WH (1971) The age of the tide and the Q of the oceans. *Deep-Sea Research* 18: 493–503.
Gladwin MT and Hart R (1985) Design parameters for borehole strain instrumentation. *Pure and Applied Geophysics* 123: 59–80.
Goodkind JM (1999) The superconducting gravimeter. *Review of Scientific Instruments* 70: 4131–4152.
Haas R and Schuh H (1998) Ocean loading observed by geodetic VLBI. In: Ducarme B and Paquet P (eds.) *Proceedings of the 13th International Symposium on Earth Tides*, pp. 111–120. Brussels: Observatoire Royal de Belgique.
Harrison JC (1971) New Programs for the Computation of Earth Tides, *Internal Technical Report*. CIRES, University of Colorado.
Harrison JC (1976) Cavity and topographic effects in tilt and strain measurement. *Journal of Geophysical Research* 81: 319–328.
Harrison JC (1985) *Earth Tides*, New York: Van Nostrand Reinhold.
Harrison JC and Herbst K (1977) Thermoelastic strains and tilts revisited. *Geophysical Research Letters* 4: 535–537.
Harrison JC and LaCoste LJB (1978) The measurement of surface gravity. In Mueller II (ed.) *Applications of Geodesy to Geodynamics: Ninth GEOP Conference*, pp. 239–243, Columbus, OH: Ohio State University. rep. 280.
Hart RHG, Gladwin MT, Gwyther RL, Agnew DC, and Wyatt FK (1996) Tidal calibration of borehole strainmeters: Removing the effects of local inhomogeneity. *Journal of Geophysical Research* 101: 25,553–25,571.
Hartmann T and Wenzel H-G (1995) The HW95 tidal potential catalogue. *Geophysical Research Letters* 22: 3553–3556.
Hatanaka Y, Sengoku A, Sato T, Johnson JM, Rocken C, and Meertens C (2001) Detection of tidal loading signals from GPS permanent array of GSI Japan. *Journal of the Geodetic Society of Japan* 47: 187–192.
Haubrich RA and Munk WH (1959) The pole tide. *Journal of Geophysical Research* 64: 2373–2388.
Herring TA, Mathews PM, and Buffett BA (2002) Modeling of nutation-precession: Very long baseline interferometry results. *Journal of Geophysical Research* 107(B4): 2069, doi:10.1029/2001JB000165.
Hewitt E and Hewitt R (1979) The Gibbs-Wilbraham phenomenon: An episode in Fourier analysis. *Archives for the History of the Exact Sciences* 21: 129–169.
Hinderer J, Florsch N, Maekinen J, Legros H, and Faller JE (1991) On the calibration of a superconducting gravimeter using absolute gravity measurements. *Geophysical Journal International* 106: 491–497.
Itsueli UJ, Bilham R, Goulty NR, and King GCP (1975) Tidal strain enhancement observed across a tunnel. *Geophysical Journal of the Royal Astronomical Society* 42: 555–564.
Iwano S, Fukuda Y, Sato T, Tamura Y, Matsumoto K, and Shibuya K (2005) Long-period tidal factors at Antarctica Syowa Station determined from 10 years of superconducting gravimeter data. *Journal of Geophysical Research* 110: B10,403, doi:10.1029/2004JB003551.
Jeffreys H (1976) *The Earth: Its Origin, History and Physical Constitution*. Cambridge: Cambridge University Press.
Jeffreys H and Vincente RO (1957) The theory of nutation and the variation of latitude. *Monthly Notices of the Royal Astronomical Society* 117: 142–161.
Jentzsch G (1997) Earth tides and Ocean tidal loading. In: Wilhelm H, Zürn W, and Wenzel HG (eds.) *Tidal Phenomena*, pp. 145–171. Berlin: Springer-Verlag.
Jentzsch G (2006) Proceedings of the 15th International Symposium on Earth Tides. *Journal of Geodynamics* 41: 1–4.
Kamigaichi O (1998) Green functions for the earth at borehole installation sensor depths for surface point load. *Papers in Meteorology and Geophysics* 48: 89–100.
Khan SA and Scherneck HG (2003) The M_2 ocean tide loading wave in Alaska: Vertical and horizontal displacements, modelled and observed. *Journal of Geodesy* 77: 117–127, doi:10.1007/s00190-003-0312-y.
King GCP and Bilham R (1973) Tidal tilt measurement in Europe. *Nature* 243: 74–75.
King GCP, Zürn W, Evans R, and Emter D (1976) Site correction for long-period seismometers, tiltmeters, and strainmeters. *Geophysical Journal of the Royal Astronomical Society* 44: 405–411.
King M (2006) Kinematic and static GPS techniques for estimating tidal displacements with application to Antarctica. *Journal of Geodynamics* 41: 77–86.
King MA and Padman L (2005) Accuracy assessment of ocean tide models around Antarctica. *Geophysical Research Letters* 32: L23,608, doi:10.1029/2005GL023901.
Kohl ML and Levine J (1995) Measurement and interpretation of tidal tilts in a small array. *Journal of Geophysical Research* 100: 3929–41.
Ku LF, Greenberg DA, Garrett C, and Dobson FW (1985) The nodal modulation of the M_2 tide in the Bay of Fundy and Gulf of Maine. *Science* 230: 69–71.
Kudryavtsev SM (2004) Improved harmonic development of the Earth tide-generating potential. *Journal of Geodesy* 77: 829–838.
Lambert A (1974) Earth tide analysis and prediction by the response method. *Journal of Geophysical Research* 79: 4952–4960.
Le Provost C, Bennett AF, and Cartwright DE (1995) Ocean tides for and from TOPEX / POSEIDON. *Science* 267: 639–642.
Le Provost C, Lyard F, and Molines J (1991) Improving ocean tide predictions by using additional semidiurnal constituents from spline interpolation in the frequency domain. *Geophysical Research Letters* 18: 845–848.
Le Provost C, Lyard F, Molines JM, and Genco ML (1998) A hydrodynamic ocean tide model improved by assimilating a satellite altimeter-derived data set. *Journal of Geophysical Research* 103: 5513–5529.
Levine J, Meertens C, and Busby R (1989) Tilt observations using borehole tiltmeters: 1. Analysis of tidal and secular tilt. *Journal of Geophysical Research* 94: 574–586.
Llubes M and Mazzega P (1997) Testing recent global ocean tide models with loading gravimetric data. *Progress in Oceanography* 40: 369–383.
Longman IM (1959) Formulas for computing the tidal accelerations due to the Moon and the Sun. *Journal of Geophysical Research* 64: 2351–2355.
Love AEH (1911) *Some Problems of Geodynamics*. Cambridge: Cambridge University Press.
Mathews PM and Guo JY (2005) Viscoelectromagnetic coupling in precession-nutation theory. *Journal of Geophysical Research* 110(B2): B02402, doi:10.1029/2003JB002915.
Mathews PM, Buffett BA, and Shapiro II (1995a) Love numbers for diurnal tides: Relation to wobble admittances and resonance expansion. *Journal of Geophysical Research* 100: 9935–9948.
Mathews PM, Buffett BA, and Shapiro II (1995b) Love numbers for a rotating spheroidal Earth: New definitions and numerical values. *Geophysical Research Letters* 22: 579–582, doi:10.1029/95GL00161.
Mathews PM, Dehant V, and Gipson JM (1997) Tidal station displacements. *Journal of Geophysical Research* 102: 20,469–20,477.
Mathews PM, Herring TA, and Buffett BA (2002) Modeling of nutation and precession: New nutation series for nonrigid

Earth and insights into the Earth's interior. *Journal of Geophysical Research* 107(B4): 2068, doi:10.1029/2001JB000390.

Matsumoto K, Sato T, Takanezawa T, and Ooe M (2001) GOTIC2: A program for computation of oceanic tidal loading effect. *Publications of the International Latitude Observatory, Mizusawa* 47: 243–248.

McCarthy DD and Pétit G (2004) IERS Conventions (2003) *IERS Technical Note 32*. Frankfurt am Main: Verlag des Bundesamts für Kartographic und Geodäsic.

Meertens C, Levine J, and Busby R (1989) Tilt observations using borehole tiltmeters: 2, analysis of data from Yellowstone National Park. *Journal of Geophysical Research* 94: 587–602.

Meertens CM and Wahr JM (1986) Topographic effect on tilt, strain, and displacement measurements. *Journal of Geophysical Research* 91: 14057–14062.

Melchior P (1983) *The Tides of the Planet Earth*. New York: Pergamon.

Merriam JB (1980) The series computation of the gravitational perturbation due to an ocean tide. *Physics of the Earth and Planetary Interiors* 23: 81–86.

Merriam JB (1985) Toroidal Love numbers and transverse stress at the Earth's surface. *Journal of Geophysical Research* 90: 7795–7802.

Merriam JB (1986) Transverse stress Green's functions. *Journal of Geophysical Research* 91: 13,903–13,913.

Merriam JB (1992) An ephemeris for gravity tide predictions at the nanogal level. *Geophysical Journal International* 108: 415–422.

Merriam JB (1995) Non-linear tides observed with the superconducting gravimeter. *Geophysical Journal International* 123: 529–540.

Merriam JB (2000) The response method applied to the analysis of superconducting gravimeter data. *Physics of the Earth and Planetary Interiors* 121: 289–299.

Miller SP and Wunsch C (1973) The pole tide. *Nature Physical Science* 246: 98–102.

Mitrovica JX, Davis JL, and Shapiro II (1994) A spectral formalism for computing three-dimensional deformations due to surface loads, 1, theory. *Journal of Geophysical Research* 99: 7057–7074.

Molodenskii MS (1961) The theory of nutations and diurnal earth tides. *Communications de l' Observatoire Royal de Belgique, Series Geophysique* 58: 25–56.

Mueller G (1977) Thermoelastic deformations of a half-space: A Green's function approach. *Journal of Geophysics* 43: 761–769.

Munk WH and Cartwright DE (1966) Tidal spectroscopy and prediction. *Philosophical Transactions of the Royal Society Series A* 259: 533–581.

Munk WH and Hasselmann K (1964) Super-resolution of tides. In: Yoshida K (ed.) *Studies on Oceanography; A Collection of Papers Dedicated to Koji Hidaka in Commemeration of his Sixtieth Birthday*, pp. 339–344. Tokyo: University of Tokyo Press.

Munk WH, Zetler BD, and Groves GW (1965) Tidal cusps. *Geophysical Journal* 10: 211–219.

Neuberg J, Hinderer J, and Zurn W (1987) Stacking gravity tide observations in central Europe for the retrieval of the complex eigenfrequency of the Nearly Diurnal Free Wobble. *Geophysical Journal of the Royal Astronomical Society* 91: 853–868.

Pagiatakis SD (1990) The response of a realistic Earth to ocean tide loading. *Geophysical Journal International* 103: 541–560.

Pawlowicz R, Beardsley B, and Lentz S (2002) Classical tidal harmonic analysis including error estimates in MATLAB using T_TIDE, *Computers and Geosciences* 28: 929–937.

Penna NT and Stewart MP (2003) Aliased tidal signatures in continuous GPS height time series. *Geophysical Research Letters* 30: SDE 1–1, doi:10.1029/2003GL018828.

Petrov L and Ma C (2003) Study of harmonic site position variations determined by very long baseline interferometry. *Journal of Geophysical Research* 108: ETG 5–1, doi:10.1029/2002JB001801.

Ponchaut F, Lyard F, and LeProvost C (2001) An analysis of the tidal signal in the WOCE sea level dataset. *Journal of Atmospheric and Oceanic Technology* 18: 77–91.

Ray RD (1998) Ocean self-attraction and loading in numerical tidal models. *Marine Geodesy* 21: 181–192.

Ray RD (2001) Resonant third-degree diurnal tides in the seas off Western Europe. *Journal of Physical Oceanography* 31: 3581–3586.

Ray RD and Egbert GD (2004) The global S_1 tide. *Journal of Physical Oceanography* 34: 1922–1935.

Ray RD and Ponte RM (2003) Barometric tides from ECMWF operational analyses. *Annales Geophysicae.* 21: 1897–1910.

Ray RD and Poulose S (2005) Terdiurnal surface-pressure oscillations over the continental United States. *Monthly Weather Review* 133: 2526–2534.

Ray RD and Sanchez BV (1989) Radial deformation of the earth by oceanic tidal loading. *NASA Technical Memorandum*, *TM-100743*, Goddard Space Flight Center, Greenbelt, MD.

Ray RD, Eanes RJ, and Lemoine FG (2001) Constraints on energy dissipation in the Earth's body tide from satellite tracking and altimetry. *Geophysical Journal International* 144: 471–480.

Richter B, Wilmes H, and Nowak I (1995) The Frankfurt calibration system for relative gravimeters. *Metrologia* 32: 217–223.

Roosbeek F (1995) RATGP95: a harmonic development of the tide-generating potential using an analytical method. *Geophysical Journal International* 126: 197–204.

Rosat S, Hinderer J, Crossley D, and Boy JP (2004) Performance of superconducting gravimeters from long-period seismology to tides. *Journal of Geodynamics* 38: 461–476.

Sato T and Harrison JC (1990) Local effects on tidal strain measurements at Esashi, Japan. *Geophysical Journal International* 102: 513–526.

Sato T, Tamura Y, Higashi T, *et al.* (1994) Resonance parameters of the free core nutation measured from three superconducting gravimeters in Japan. *Journal of Geomagnetism and Geoelectricity* 46: 571–586.

Sato T, Tamura Y, Matsumoto K, Imanishi Y, and McQueen H (2004) Parameters of the fluid core resonance inferred from superconducting gravimeter data. *Journal of Geodynamics* 38: 375–389.

Schenewerk MS, Marshall J, and Dillinger W (2001) Vertical ocean-loading deformations derived from a global GPS network. 47: 237–242.

Schreiber KU, Klugel T, and Stedman GE (2003) Earth tide and tilt detection by a ring laser gyroscope. *Journal of Geophysical Research* 108: doi:10.1029/2001JB000569.

Shum CK, Woodworth PL, Andersen GD, *et al.* (1997) Accuracy assessment of recent ocean tide models. *Journal of Geophysical Research* 102: 25,173–25,194.

Smith ML and Dahlen FA (1981) The period and Q of the Chandler wobble. *Geophysical Journal of the Royal Astronomical Society* 64: 223–281.

Sovers OJ (1994) Vertical ocean loading amplitudes from VLBI measurements. *Geophysical Research Letters* 21: 357–360.

Standish EM, Newhall XX, Williams JG, and Yeomans DK (1992) Orbital ephemerides of the Sun, Moon and planets. In: Seidelmann PK (eds.) *Explanatory Supplement to the Astronomical Almanac*, pp. 279–323. Sausalito, California: University Science Books.

Takemoto S (1981) Effects of local inhomogeneities on tidal strain measurements. *Bulletin of the Disaster Prevention Research Institute of Kyoto University* 31: 211–237.

Tamura Y (1982) A computer program for calculating the tide generating force. *Publications of the International Lattitude Observatory, Mizusawa* 16: 1–20.

Tamura Y (1987) A harmonic development of the tide-generating potential. *Bulletin d'Information des Marées Terrestres* 99: 6813–6855.

Tamura Y, Sato T, Fukuda Y, and Higashi T (2005) Scale factor calibration of a superconducting gravimeter at Esashi Station, Japan, using absolute gravity measurements. *Journal of Geodesy* 78: 481–488.

Tamura Y, Sato T, Ooe M, and Ishiguro M (1991) A procedure for tidal analysis with a Bayesian information criterion. *Geophysical Journal International* 104: 507–516.

Torge W (1989) *Gravimetry*. Berlin: Walter de Gruyter Verlag.

Trupin A and Wahr J (1990) Spectroscopic analysis of global tide gauge sea level data. *Geophysical Journal International* 100: 441–453.

Van Camp M and Vauterin P (2005) Tsoft: Graphical and interactive software for the analysis of time series and Earth tides. *Computers and Geosciences* 31: 631–640.

Wahr JM (1981a) Body tides on an elliptical, rotating, elastic and oceanless Earth. *Geophysical Journal of the Royal Astronomical Society* 64: 677–703.

Wahr JM (1981b) A normal mode expansion for the forced response of a rotating Earth. *Geophysical Journal of the Royal Astronomical Society* 64: 651–675.

Wahr JM (1985) Deformation induced by polar motion. *Journal of Geophysical Research* 90: 9363–9368.

Wahr JM and Bergen Z (1986) The effects of mantle and anelasticity on nutations, earth tides, and tidal variations in rotation rate. *Geophysical Journal* 87: 633–668.

Wahr JM and Sasao T (1981) A diurnal resonance in the ocean tide and in the Earth's load response due to the resonant free 'core nutation'. *Geophysical Journal of the Royal Astronomical Society* 64: 747–765.

Wang R (1997) Tidal response of the solid Earth. In: Wilhelm H, Zürn W, and Wenzel HG (eds.) *Tidal Phenomena*, pp. 27–57. Berlin: Springer-Verlag.

Warburton RJ and Goodkind JM (1976) Search for evidence of a preferred reference frame. *Astrophysical Journal* 208: 881–886.

Wenzel H-G (1996) The nanogal software: earth tide data processing package ETERNA 3.3, *Bulletin d'Information des MaréesTerrestres*124 : 9425 – –9439.

Wessel P and Smith WHF (1996) A global, self-consistent, hierarchical, high-resolution shoreline database. *Journal of Geophysical Research* 101: 8741–8743.

Wilhelm H (1983) Earth's flattening effect on the tidal forcing field. *Journal of Geophysics* 52: 131–135.

Wilhelm H (1986) Spheroidal and torsional stress coefficients. *Journal of Geophysics* 55: 423–432.

Wilhelm H, Zürn W, and Wenzel HG (1997) *Tidal Phenomena*. Berlin: Springer-Verlag.

Xi Q (1987) A new complete development of the tide-generating potential for the epoch J2000.0. *Bulletin d'Information des Marées Terrestres* 99: 6766–6812.

Zürn W (1997) The nearly-diurnal free wobble-resonance. In: Wilhelm H, Zürn W, and Wenzel HG (eds.) *Tidal Phenomena*, pp. 95–109. Berlin: Springer-Verlag.

Zürn W, Rydelek PA, and Richter B (1986) The core-resonance effect in the record from the superconducting gravimeter at Bad Homburg. In: Viera R (eds.) *Proceedings of the 10th International Symposium on Earth Tides*, pp. 141–147. Madrid: Consejo Superior de Investigaciones Cientificas.